Ameliorating quercetin constraints in cancer therapy with pH-responsive agarose-polyvinylpyrrolidone -hydroxyapatite nanocomposite encapsulated in double nanoemulsion

Samadi, Amirmasoud; Pourmadadi, Mehrab; Yazdian, Fatemeh; Rashedi, Hamid; Navaei-Nigjeh, Mona; da Silva, Tatiane Eufrásio

Published in:
International Journal of Biological Macromolecules

Link to article, DOI:
10.1016/j.ijbiomac.2021.03.146

Publication date:
2021

Document Version
Peer reviewed version

Ameliorating quercetin constraints in cancer therapy with pH-responsive agarose-polyvinylpyrrolidone -hydroxyapatite nanocomposite encapsulated in double nanoemulsion

Amirmasoud Samadi, Mehrab Pourmadadi, Fatemeh Yazdian, Hamid Rashedi, Mona Navaei-Nigjeh, Tatiane Eufrasio-da-silva

PII: S0141-8130(21)00690-5

DOI: https://doi.org/10.1016/j.ijbiomac.2021.03.146

Reference: BIOMAC 18192

To appear in: *International Journal of Biological Macromolecules*

Received date: 26 December 2020

Revised date: 23 February 2021

Accepted date: 23 March 2021

Please cite this article as: A. Samadi, M. Pourmadadi, F. Yazdian, et al., Ameliorating quercetin constraints in cancer therapy with pH-responsive agarose-polyvinylpyrrolidone -hydroxyapatite nanocomposite encapsulated in double nanoemulsion, *International Journal of Biological Macromolecules* (2018), https://doi.org/10.1016/j.ijbiomac.2021.03.146

Ameliorating quercetin constraints in cancer therapy with pH-responsive agarose-polyvinylpyrrolidone -hydroxyapatite nanocomposite encapsulated in double nanoemulsion

Amirmasoud Samadi[a], Mehrab Pourmadadi [a], Fatemeh Yazdian[b], Hamid Rashedi[a], Mona Navaei-Nigjeh[c], Tatiane Eufrasio-da-silva [d, e]

[a] Department of Biotechnology, School of Chemical Engineering, College of Engineering, University of Tehran, Tehran, Iran

[b] Department of Life Science Engineering, Faculty of New Science and Technologies, University of Tehran, Tehran, Iran

[c] Pharmaceutical Sciences Research Center, The Institute of Pharmaceutical Sciences (TIPS), Tehran University of Medical Sciences, Tehran, Iran

[d] Department of Health Technology, Technical University of Denmark (DTU), 2800 Kgs. Lyngby, Denmark.

[e] Radboud university medical center, Radboud Institute for Molecular Life Sciences, Department of Dentistry - Regenerative Biomaterials, Philips van Leydenlaan 25, 6525EX Nijmegen, The Netherlands

Corresponding Authors: Fatemeh Yazdian, Department of Life Science Engineering, Faculty of New Science and Technologies, University of Tehran, Tehran, Iran

Hamid Rashedi, Department of Biotechnology, School of Chemical Engineering, College of Engineering, University of Tehran, Tehran, Iran

Email : yazdian@ut.ac.ir

hrashedi@ut.ac.ir

Abstract

Despite quercetin (QC) promising features for cancer therapy, low solubility, poor permeability, and short biological half-life time significantly confine its application in cancer therapy. In this study, a novel approach is developed to improve loading efficiency and attain quercetin sustained-release concurrently. In this direction, hydrogel nanocomposite of agarose (AG)-polyvinylpyrrolidone (PVP) hydroxyapatite (HAp) was loaded with QC. Incorporating HAp nanoparticles in the AG-PVP hydrogel improved the loading efficiency up to 61%. Also, the interactions between nanoparticle, drug, and hydrogel polymers rendered the nanocomposite pH-responsive at acidic conditions and controlled the burst release at neutral conditions. Then, QC-loaded hydrogel was encapsulated into the water in oil in water nanoemulsions to further sustain the drug release. As a result, the pH-responsive release of QC with prolonged-release over 96 h was observed. In more detail, according to the Korsmeyer-Peppas mathematical model, the mechanism of release was anomalous (diffusion-controlled) at pH 7.4 and anomalous transport(dissolution-controlled) at pH 5.4. The presence of all nanocomposite components was confirmed with FTIR analysis, and XRD results approved the incorporation of QC in the fabricated nanocomposite. The homogeneous surface of the nanocomposite in FESEM images showed good compatibility between components. The zeta potential analysis confirmed the good stability of the nanocarriers. Besides, the fabricated AG-PVP-HAp-QC platform showed significant cytotoxicity on MCF-7 cells compared to QC as a free drug ($p<0.001$) and to quercetin-loaded AG-PVP (AG-PVP-QC) ($p<0.001$) with enhanced apoptosis induction after the

addition of HAp. Accordingly, this delivery platform ameliorated loading and sustained-release of QC, as well as its anticancer activity by releasing the drug at an effective therapeutic level over a long period to induce apoptosis. Thus, turning this drug delivery system into a potential candidate for further biomedical applications.

Keywords: Quercetin, Hydroxyapatite, pH-responsive nanocarrier, sustained-release, anticancer activity

Abbreviations

AG: Agarose
PVP: Polyvinylpyrrolidone
HAp: Hydroxyapatite
QC: Quercetin
PVA: Polyvinyl alcohol
PEG: Polyethylene glycol
TC: Tamoxifen citrate
ZNO: Zinc oxide
FBS: Fetal bovine serum
BSA: Bovine serum albumin
PBS: Phosphate buffer saline
DMSO: dimethylsulfoxide
EDTA: Ethylenediaminetetraacetic acid
DMEM: Dulbecco's Modified Eagle's Medium
MTT: 3-(4, 5-dimethyl-thiazol-2-yl)-2, 5- diphenyl-tetrazolium bromide
ATCC: American Type Culture Collection
FESEM: Field Emission Scanning Electron Microscope
FTIR: Fourier transform infrared
DLS: Dynamic light scattering
PDI: Polydispersity Index
XRD: X-ray diffraction
FWHM: Full width at half maximum
PI: Propidium Iodide
FITC: Fluorescein isothiocyanate
SEM: standard error of the mean

1. Introduction

Over the last century, cancer cases have increased at an alarming pace. Among cancer cases, breast cancer has increased drastically globally, with over 1.5-1.7 million new confirmed cases worldwide every year [1]. Indeed, breast cancer is currently the second dominant cause of death among females in the world. In the United States alone, breast cancer was responsible for more than forty thousand deaths in 2019 [2]. Several therapeutics have been proposed, including chemotherapy, to tackle this dismaying global challenge; nevertheless, the effectual application of chemotherapy is restrained due to multiple drug resistance (MDR), toxicity, nonspecific distribution, and poor physicochemical properties. Accordingly, the furtherance of treatment methods at the movement is to develop safe methods based on natural compounds with less

toxicity and (or) fewer side effects as a requisite to overcome barriers faced in cancer drug therapy [1]; to this end, the use of naturally derived polyphenols has attracted further attention recently [3].

Quercetin (QC), a plant flavonol from the flavonoid group of polyphenols, is amply present in various plants, foods, and drinks [1]. Quercetin has broad biological activities, namely antiviral [4], anti-inflammatory [5], anti-tyrosinase [6], and antitumor effect through induction of ROS-dependent pathway in MCF-7 cells [1]. It also presents a wide range of physiological activities, like free radical scavenging and regulating the expression of pro-inflammatory cytokines [7]. Upregulation of the hemeoxygenase-1 pathway and downregulation of the nuclear factor kappa B pathway are among other quercetin physiological activities. Also, impeding the mobility of breast cancer cells to contain tumor progression through suppression of migration marker proteins, such as matrix metalloproteinases (e.g., MMP-2 and MMP-9) and vascular endothelial growth factor (VEGF) are among other outstanding activities imputed to quercetin [8,9]. Moreover, quercetin is employed as a chemosensitizer along with chemotherapeutic drugs to alleviate multidrug resistance of breast cancer cells through inhibition of P-glycoprotein (Pgp) expression [10,11].

Despite the promising features described above, the following intrinsic properties, such as low solubility, poor permeability, and short biological half-life—which results in low bioavailability—are some of the significant drawbacks that hinder the application of quercetin as an anticancer drug [12]. Entrapment of quercetin into biodegradable polymeric carriers could be an appropriate and beneficial approach to overcome these limitations. Hydrogels are one of the ubiquitous tools prepared either by synthetic polymers (e.g., Polyethylene glycol (PEG), Polyvinyl alcohol (PVA), and Polyvinylpyrrolidone (PVP)) or natural polymers (e.g., chitosan, hyaluronic acid, gelatin, collagen, alginate, and agarose) to produce biodegradable, biocompatible, non-toxic and non-immunogenic polymeric carriers [13]. Among many synthetic-based hydrogel formers, Polyvinylpyrrolidone (PVP) is a water-soluble polymer made from N-vinylpyrrolidone monomers, and it is recognized as safe for pharmaceutical applications by the US Food and Drug Administration (FDA) [14]. Also, PVP has been used as a stabilizer agent for prepared nanocarriers or a crosslinker of polymer networks [15]. It has recently been employed for hydrogel nanocomposites preparation due to its biocompatibility [16]. Besides, among many natural-based hydrogel formers, agarose (AG) is a biocompatible and non-toxic polysaccharide with a porous nature derived from red algae [17]. It is made of d-galactose-3,6-anhydro-l-galactopyranose repeat units. The physical crosslinking property of AG during hydrogel formation leads to a lack of reactive chemistry and effectuation capability, making AG a more attractive candidate than PEG and alginate, which both have these shortcomings. Furthermore, agarose-based compounds have been used to provide pH-sensitive features to hydrogels [18]. These attributes contribute to the capability of agarose as a suitable substance for controlled drug delivery applications.

Regarding stimuli-responsive platforms as a promising option for targeted drug delivery, it is known that several stimuli can be employed. For instance, pH-value is at the moment used for such purposes. It is also known that cancerous tissues exhibit different pH than that of healthy tissues [19]. Lower extracellular pH in tumor cells has been detected as a consequence of the rapid proliferation of cancer cells that leads to an inadequate amount of oxygen and the production of lactic acid through glycolysis. This effect, known as the Warburg effect, has inspired the use of pH-responsive drug delivery systems [20]. pH-responsive hydrogels

contribute significantly to the controlled delivery of drugs and biomedical applications [18]. In a recent study, a pH-sensitive agarose-PVA hydrogel nanocomposite incorporated with carbon dots was developed for the delivery of Norfloxacin as an antibacterial agent [21]. Moreover, the use of pH-responsive platforms is not confined to the release of drugs at acidic conditions. For instance, electrosprayed hydrophilic nanocomposites coated with shellac were developed for colon-specific delayed delivery of tamoxifen citrate (TC). Tamoxifen citrate is a poorly water-soluble drug for recurrent metastatic breast cancer treatment. In the oral administration of this drug, it is required to protect the drug from release in the acidic condition of the stomach. TC controlled-release was attained by coating nanocomposites with a shellac layer which prevents the drug release at the acidic conditions and quickly dissolves at neutral conditions to release TC in the colon [22]. Also, the use of core-shell nanofibers fabricated by electrospinning is another example of pH-sensitive release at the neutral conditions in the oral administration of therapeutics [23].

Despite the discussed benefits of using hydrogels for drug delivery, defects of hydrogel systems like low homogeneity, lack of multiresponsiveness, and poor loading of hydrophobic drugs in hydrogels due to their hydrophilic nature impede their extensive application. The addition of nanoparticles to hydrogels addresses the mentioned defects and paves the way for a wider application of hydrogels for drug delivery [24]. Reduced particle size, high surface area, controlled shape, and ability to incorporate hydrophobic molecules along with magnetic, thermal, and electrical properties that can be employed for responsive release of encapsulated drugs are among reasons that render hydrogel nanocomposites a promising candidate for stimuli-responsive targeted drug delivery [25]. In this direction, hydroxyapatite (HAp), a calcium phosphate derived mineral with morphology and composition resembling human hard tissues, well known for its high biocompatibility and drug-loading efficiency without immunogenic response, is a desirable nanoparticle for inclusion in hydrogels to provide the mentioned features to hydrogels. It is a prominent drug delivery tool due to its biodegradability, which obviates safety issues. It has been employed for the delivery of hydrophobic drugs [26], and control burst release from hydrogels [27]. Moreover, hydroxyapatite nanoparticles have demonstrated an inhibitory effect on the proliferation of tumor cells through the activation of mitochondrial-dependent apoptosis and stimulated immune response [28].

In this study, agarose and polyvinylpyrrolidone polymers with hydroxyapatite (HAp) nanoparticles were used to prepare a hydrogel nanocomposite loaded with quercetin. The polar nature of PVP due to its carbonyl group and hydroxyl groups in agarose facilitates hydrogen bonds forming between polymers, HAp nanoparticles, and the model drug [29–31]. These interactions, along with affording high surface area by HAp nanoparticles leads to enhanced loading of QC in the fabricated hydrogel. Furthermore, alteration of the mentioned molecular interactions at acidic conditions bestows pH-responsive property to the fabricated hydrogel nanocomposite. Indeed, at acidic conditions, the dissolution of HAp is accelerated [32]. This dissolution, along with the protonation of carbonyl groups in PVP and hydroxyl groups in QC and agarose, provides repulsive forces between components. This accelerated dissolution leads to increased release at acidic conditions. In contrast, the physical and chemical interactions between the drug and components maintain nanocomposite integrity and prevent burst release of the drug at neutral conditions.

Afterward, a double nanoemulsion of water in oil in water (W/O/W) was produced according

to previously reported protocols in the literature [33] to prepare nanocarriers that contain drug-loaded hydrogel nanocomposites. The incorporation of the drug-loaded hydrogels in these nanoemulsions can prolong the release period. This is because, in W/O/W emulsions, the internal and external aqueous phases are separated by an oil layer. This oil layer acts as a liquid membrane to control the release of the hydrophobic drug quercetin from the internal phase to the external phase [34]. The formation of this double emulsion with nano size is mainly relying on the formation of water in oil primary emulsion, which is further emulsified in another aqueous solution. The primary emulsion is formed using a lipophilic emulsifier to stabilize the interaction between drug-loaded hydrogel nanocomposites and oil as a disperse phase (W/O). In the second step, a hydrophilic surfactant maintains the interaction between the new interface of oil/water (O/W).

Therefore, this study aimed to load quercetin into a hydrogel nanocomposite of AG-PVP-HAp and incorporate it in the internal aqueous phase of a W/O/W double emulsion to develop a pH-responsive drug delivery system with an enhanced drug loading and a sustained release profile in order to investigate its *in vitro* antitumor effect on MCF-7 breast cancer cells as a method to validate its efficiency as a drug delivery system to treat cancer. To the best of our knowledge, this is a novel approach to address prevalent drawbacks of treating cancer cells with quercetin by concurrently augmenting loading capacity, sustained-release, and apoptosis induction effects of QC compared to free QC as the model drug. Moreover, despite the fact this novel approach aimed to treat MCF-7 breast cancer cells, its validity and utilization can lay far beyond, and its prospective use even could be applied to treat other types of cancers and localized diseases.

Materials and methods

2.1. Materials

MCF-7 human breast cancer cell line was obtained from American Type Culture Collection (ATCC) (Manassas, VA). Dulbecco's Modified Eagle's Medium (DMEM) High Glucose was purchased from Hy Clone Thermo Scientific. Fetal bovine serum (FBS) was obtained from Gibco-Life Technologies. Penicillin/streptomycin and 0.25% (w/v) trypsin–0.1% (w/v) Ethylenediaminetetraacetic acid (EDTA) were purchased from Solarbio (Beijing Solarbio Science and Technology, China). 3-(4, 5-dimethyl-thiazol-2-yl)-2, 5- diphenyl-tetrazolium bromide (MTT) and dimethylsulfoxide (DMSO) were purchased from Sigma (USA). Culture flasks and dishes were from Corning (Corning, NY, USA).

Phosphate buffer saline (PBS) was obtained from the Iranian Research Organization for Science and Technology (IROST). Polyvinylpyrrolidone (PVP K90, 1,200,000 Daltons), agarose (AG) pharmaceutical grade type I low EEO (suitable for hydrogel preparation), hydroxyapatite (HAp) ($Ca_{10}(PO_4)_6(OH)_2$, 1004.6 g/mol), and quercetin (QC) (3,3′,4′,5,7- pentahydroxyflavone) were purchased from Sigma-Aldrich. Span 80 and paraffin oil were obtained from Merck and Carlo Erba Reagents, respectively. Glyoxal and Polyvinyl alcohol (PVA) were obtained from Sigma-Aldrich.

2.2. Preparation of AG-PVP-HAp hydrogel

Initially, polyvinylpyrrolidone (PVP) was gradually added to 30 mL of deionized water under magnetic stirring (~500 rpm) at room temperature to obtain a 5% w/v solution. Then, 2.5% w/v of agarose (AG) was added to the PVP solution, and vigorously stirred. Hydroxyapatite (1% w/v) was added to the AG-PVP hydrogel in this step. The addition of HAp to the prepared hydrogel of AG-PVP results in physical entanglement and formation of non-covalent bonds between polymers functional groups and HAp as well as QC added in the next step [25]. These

interactions improve quercetin loading as a hydrophobic drug.

2.3. Quercetin loading and entrapment in the AG-PVP-HAp hydrogel

Quercetin (QC) was initially dissolved in ethanol due to its hydrophobic nature prior to loading into the prepared AG-PVP-HAp hydrogel nanocomposite. Then, the dissolved quercetin (100 µg mL^{-1}) was added to the hydrogel. It was carried out by a drop-by-drop loading of quercetin under vigorous stirring. After the addition of the drug, glyoxal with 0.1% v/v concentration was used as a gelator (crosslinker) to form a homogenous AG-PVP hydrogel that incorporates nanoparticles and quercetin within itself. Finally, a hydrogel incorporating nanoparticles bonded to the polymers and quercetin within this structure is formed, as shown in Fig. 1.

2.4. Preparing double emulsion

After preparing the QC-loaded hydrogel nanocomposite, the nanocomposite was loaded into the internal phase of a W/O/W double emulsion to improve the sustained-release further. The primary emulsion was formed by emulsification of the aqueous phase, including hydrogel in an oil phase. 20 mL of the quercetin-loaded hydrogel nanocomposite was gradually added under high-speed stirring to the hydrophobic phase containing 30 mL of paraffin oil with 20% v/v Span 80 as surfactant agent. After 10 min, the hydrophilic phase containing 30 mL PVA 1% v/v was slowly added to the produced primary emulsion under stirring. After 10 min, the suspension was removed from the stirrer, and phases were separated. Due to the lower density of the hydrophobic phase than the hydrophilic phase, the hydrophobic phase was separated from above the hydrophilic phase. After removing the hydrophobic phase, the remaining hydrophilic phase containing prepared double emulsions was centrifuged (Hermle-Labnet) at 4500 rpm for 5 min to separate the fabricated double emulsions. In Fig. 2, the schematics of oil in water (O/W) and water in oil in water (W/O/W) double emulsions encapsulating hydrogel nanocomposites are presented. The nanocomposite hydrogel's preparation steps and its encapsulation in the double nanoemulsion are depicted in Fig. 3.

2.5. Quercetin loading and entrapment efficiency determination

The efficiency of drug loading and entrapment for quercetin was calculated to assess the impact of incorporating HAp nanoparticles in AG-PVP hydrogel. Lyophilized nanocarriers of AG-PVP-QC (1 mg) and AG-PVP-HAp-QC (1 mg) were dispersed in 1 mL of PBS, next 1 mL of organic solvent ethyl acetate was added. The mixtures were agitated, and the ethyl acetate phase was separated. The free content of QC in the ethyl acetate phase was determined for each sample using a UV-Vis spectrophotometer at 370 nm [35]. The percentages of quercetin entrapment (or encapsulation) efficiency and loading efficiency were calculated by equations 1 and 2 [36], respectively. The tests were conducted in triplicate for each group (with or without HAp).

$$\text{Entrapment Efficiency (\%)} = \frac{\text{(Total amount of Quercetin) - (Free amount of Quercetin)}}{\text{(Total amount of Quercetin)}} \quad \text{Eq}_1$$

$$\text{Loading Efficiency (\%)} = \frac{\text{(Total amount of Quercetin)-(Free amount of Quercetin)}}{\text{(Total amount of Nanocomposite)}} \quad \text{Eq}_2$$

2.6. Characterization of the fabricated platform

The average size distribution of nanoemulsions and their surface charge (zeta potential) were determined by Dynamic light scattering (DLS) analyzer and zeta potential measurement, respectively, using a Horiba SZ-100 Zeta analyzer (HORIBA Scientific, Kyoto, Japan). The

nanocomposite's surface morphology was observed using Field Emission Scanning Electron Microscope (FESEM) (TESCAN, MIRA III model, Czech Republic) at an accelerated voltage of 30 kV. The experiments were performed at a scattering angle of 90° after probe sonication of solution. To confirm the addition of all components in the fabricated hydrogel nanocomposite, the potential interactions between components was analyzed by Fourier transform infra-red (FTIR) spectroscopy at room temperature by a KBr pellet method. 1 mg of each sample was grounded in a mortar pestle along with KBr to make a small pellet of a thickness of 0.1 cm. KBr pellet was used as blank. The scanning range of the spectrum was between 400 to 4000 cm^{-1}. The spectra of PVP, AG-PVP, AG-PVP-HAp, and AG-PVP-HAp-QC were recorded on lyophilized samples using a PerkinElmer Spectrum Version 10.03.06. The crystalline structure of the nanocomposite after the addition of each component were analyzed to affirm the complexation of hydrogel polymers with nanoparticles and the model drug. This analysis was performed by X-ray diffraction (XRD, PHILIPS, PW1730, Netherlands) in the 2θ range from 5 to 80° using a Cu Kα source with λ=1.54056. The step size was 0.05 deg, and a time per step of 1second was selected. HighScore plus 3 was used to analyze XRD diffractograms.

2.7. In vitro drug release study

The release of quercetin from nanocarriers was scrutinized using the dialysis method [37] at two different phosphate buffer mediums (pH 7.4 and 5.4) in a water bath at 37 °C to assess pH responsive attribute of the delivery platform and sustained-release of QC. Nanocarriers containing AG-PVP-HAp-QC and AG-PVP-QC (1 mL for each) were transferred into dialysis bags (Mw cutoff 12000 g mol^{-1}) and immersed in 50 mL of phosphate buffer containing ethanol 20 % v/v (pH 7.4 and pH 5.4) at 37 °C. To assess the double emulsion impact on the sustained-release at pH 5.4, quercetin release from AG-PVP-HAp hydrogel not incorporated in the double emulsion was also studied.

At specified time intervals of 0, 12, 13, 24, 48, 72, and 96 hours, 300 µL of samples were taken out and replaced with an equivalent volume of fresh PBS containing ethanol 20 % v/v. The released quercetin content in buffer was determined by UV–Vis spectrophotometrically (U.V-T60U; PG Instrument, England) at a wavelength of 370 nm. All tests were performed three times and the amount of released quercetin was calculated using equation 3:

$$\text{Quercetin released (\%)} = \frac{[\text{Quercetin}]\text{rel}}{[\text{Quercetin}]\text{load}} * 100 \qquad Eq_3$$

Where in, [Quercetin]load is the amount of quercetin loaded in the nanocomposite incorporated in nanoemulsions, and [Quercetin]rel is the amount of quercetin released from the nanocarriers. To affirm the fabricated platform's pH-responsive release behavior, the statistical analysis (ANOVA) was conducted by comparing the release percentage of QC from AG-PVP-HAp-QC at pH 5.4 with all other groups.

2.8. Kinetics of drug release in various pH conditions

After investigating the release behavior of QC by the dialysis method, the drug release data were fitted to several release kinetic models to figure out the underlying drug release mechanism in pH 7.4 and 5.4. GraphPad 7 was used to fit the data to zero-order, first-order, Higuchi, Hixson–Crowell, and Korsmeyer–Peppas. The R square for each model was determined, and the release mechanism based on the parameters of the best-fitting regression model was ascertained in both neutral and acidic conditions. Also, only parameters likely to be a meaningful addition to the models were retained.

2.9. Cell culture

The breast cancer cell line, MCF-7, was purchased from American Type Culture Collection (ATCC) and cultured in DMEM media supplemented with 10% fetal bovine serum (FBS), penicillin (100 U mL^{-1}), streptomycin (100 µg mL^{-1}) at 37 °C in a humidified incubator supplemented with 5% carbon dioxide.

2.10. In vitro cytotoxicity assay

The cytotoxicity of samples, including free QC, QC-loaded in AG-PVP, and AG-PVP-HAp hydrogel nanocarriers, as well as nanocarriers containing AG-PVP-HAp without the model drug against MCF-7 cell line was inspected using 3-(4,5- dimethylthiazol-2-yl)-2,5-diphenyltetrazolium bromide (MTT) assay. The cells were grown in the culture media and kept at 37 °C with 5 % CO_2 in a tissue culture incubator. A growth medium containing 2×10^4 cells was placed in each well of a 96-well plate and incubated overnight to allow cell attachment. After 24 h, when the cells had adhered with 70 % confluency, the cells were treated with mentioned samples at a concentration equal to 60 µg mL^{-1}. This is the concentration of QC in nanocarriers containing the drug-loaded AG-PVP-HAp hydrogels after considering the loading efficiency of QC (61%). Comparing samples at equal concentrations leads to investigate the effect of the fabricated nanocarrier on cytotoxicity through alteration in the release behavior. Control cells were cultured simultaneously in a basic medium (DMEM containing 10 % FBS and 1 % antibiotic penicillin/streptomycin) without quercetin for the same period. After 72 h, the supernatants were removed, and 50 µL of fresh DMEM was added to each well, followed by adding 50 µL of 5 mg mL^{-1} of MTT solution, and the plates were incubated for a further 3-4 h. The media was then elicited, and 150 µL DMSO was added to each well while shaking for 15 min to dissolve the formazan crystals. Optical density was read on a multi-well scanning spectrophotometer (ELISA reader) at 570 nm. All tests were performed in triplicate. The viability of the treatment groups was expressed as the percentage of control, which was put on 100%. The mean and the standard error of the mean (SEM) of cell viability for each treatment was determined. The statistical analysis between groups was performed by GraphPad InStat 3 by comparing the mean, standard error of the mean, and the number of replicates (N=3) in each group.

2.11 Cell apoptosis assay

The apoptosis and necrosis analysis induced by different groups were determined after Annexin V-FITC and Propidium Iodide (PI) double staining according to the manufacturer's protocols (ApoFlowEx® FITC Kit obtained from Exbio, Czech Republic). First, MCF-7 cells were treated for 72 h with free QC, nanoemulsions containing quercetin-loaded AG-PVP and AG-PVP-HAp hydrogels, and AG-PVP-HAp without the drug. Here again, the cells were treated with the mentioned samples at a concentration equal to 60 µg mL^{-1} due to the same reason mentioned in the previous section. By the end of the treatment, cells were harvested, washed with cold PBS, suspended in 500 µL binding buffer, and stained by five µL Annexin V-FITC and five µL PI. The cells were incubated in the dark for 15 minutes and then measured by a flow cytometer (Mindray, China). The cells were scanned for fluorescence intensity in FL-1 (FITC) and FL-3 (PI) channels. The fraction of cell populations in different quadrants was analyzed using quadrant statistics. The values shown in the lower left, lower right, upper left, and upper right quadrants of each panel represent the percentage of viable (Q4), early apoptotic (Q3),

necrotic (Q1), and late apoptotic (post-apoptotic necrotic, Q2) cells, respectively. All the above-mentioned procedure was repeated three times to investigate the improved apoptosis induction of AG-PVP-HAp-QC, owing to the sustained-release of QC and the use of nanoparticles along with QC.

3. Results and discussion

3.1. Characterization

3.1.1. Fourier transform infrared (FTIR) spectroscopy

FTIR was performed to confirm the inclusion of all components in the nanocomposite through analysis of the observed peaks denoting interactions between polyvinylpyrrolidone (PVP), agarose (AG), hydroxyapatite (HAp), and quercetin (QC) as the model drug. In the FTIR spectrum of PVP, the broad peak at 3461 cm^{-1} could be attributed to the O-H stretching present in PVP. The peak at 2954 cm^{-1} could be assigned to C-H stretching vibration. The strong and sharp band detected at 1666 cm^{-1} is assigned to C=O stretching, and is aligned with the former reported spectrums of PVP [38]. Other peaks at 1494, 1461, 1427, 1373 cm^{-1} are characteristic for the C-H deformation of the cyclic CH_2 group and are in agreement with former IR spectra of PVP in literature [38]. The band at 1286 cm^{-1} was due to C-N stretching vibrations [38]. The stretching vibration peaks attributed to C-N group of PVP are detected at 1019 and 1073 cm^{-1} in PVP and are in agreement with the FTIR spectrum of PVP in previous studies [39]. To confirm the addition of AG, the FTIR spectrum of AG-PVP was studied. This spectrum showed an additional peak at 3740 cm^{-1} that denotes O-H groups present in AG, which is in accordance with the reported results of AG FTIR spectrum in the literature [40]. Also, the C-N attributed peak at 1019 cm^{-1} was not detected, but the intensity ratio of the peak at 1073 cm^{-1} increased. This is attributed to the contribution of C-O stretch in AG as reported in the literature [41] with the C-N stretching vibration in PVP. The broad peak at 3461 cm^{-1} in PVP was shifted to 3441 cm^{-1}, probably due to changes in molecular interactions between AG and PVP. The peak at 2954 cm^{-1} showed reduced intensity possibly due to the same reason. The observed peak at 1660 cm^{-1} denoting C=O stretching in the spectrum of PVP was observed again in AG-PVP spectrum. In the spectrum of AG-PVP-HAp, the intensity ratio of the peak in the range of 1162-1168 cm^{-1} increased compared to AG-PVP spectrum. This increase is due to the contribution of P=O phosphate group present in hydroxyapatite with C-O stretch in AG, which affirms the addition of HAp to the component and the presence of AG. Also, the peak at 1660 cm^{-1} in the spectrum of pure PVP was observed again. The peak at 605 cm^{-1} in AG-PVP-HAp is expressing the presence of phosphate ion due to the addition of HAp. This peak and the peak at 472 cm^{-1} in the nanocomposite spectrum is consistent with the HAp reference spectrum [42]. Also, the peak at 3441 cm^{-1} showed increased intensity ratio. This could be assigned to the overlapping of two contributions: O-H stretching in PVP and O-H stretching in HAp [42]. Here again, the peak observed at 1660 cm^{-1} in the spectrum of pure PVP and the peak at 3740 cm^{-1} denoting O-H groups present in AG were also observed in AG-PVP-HAp with almost the same intensity to confirm the presence of AG, PVP, and HAp in AG-PVP-HAp nanocomposite.

In the spectrum of AG-PVP-HAp-QC, the intensity ratio of the peak in the range of 1162-1168 cm^{-1} reduced, which indicates the probable electrostatic interactions between the drug and polymer, which ends up in the improvement of the drug complexation with nanocomposite. Furthermore, the addition of QC to the composite is confirmed by an increase in the intensity

ratio of the peak at 1660 cm^{-1} in the spectrum of AG-PVP-HAp-QC. This could be due to the characteristic peak of quercetin around 1660 cm^{-1} assigned to C=O stretching [43] which overlaps with the former peak observed at 1660 cm^{-1} in the PVP spectrum. Other characteristic peaks like peaks around 1494, 1461, 1427, and 1375 cm^{-1} that are assigned to C-H deformation of cyclic CH_2 group showed reduced intensity. The observed peaks around 734-737 cm^{-1} and 843-845 cm^{-1} in the spectra of samples are attributed to the C-H bond in QC an in agreement with the spectrum of QC reported before [43]. The observed peak at 3740 cm^{-1} that denotes O-H groups present in AG was observed again in the AG-PVP-HAp-QC spectrum. The presence of the characteristic peaks of each component and the shift of the peak demonstrating O–H and phosphate ion peak to lower wavenumbers confirm the presence of all components in the final nanocomposite and interaction of the drug with other components in the produced nanocomposite. The FTIR spectra of mentioned samples is presented in Fig. 4.

3.1.2. X-ray diffraction analysis

The change in the crystalline structure after the addition of each component and incorporation of the crystalline QC into the nanocomposite was analyzed by XRD. The XRD patterns of PVP, AG-PVP, AG-PVP-HAp, and AG-PVP-HAp-QC are displayed in Fig.5. As seen from XRD diffractograms, the X-ray diffraction of pure PVP shows two diffuse halo peaks close to 2θ equal to 10.135°θ and 20.533°θ, which is in agreement with the values reported in the literature for pure PVP and can be attributed to the amorphous nature of pure PVP [44]. In the XRD pattern of AG-PVP, the broad peak at 20.533°θ was observed. Agarose has a semi-crystalline structure owing to the hydrogen bonding formation with a broad hump around 18-29°θ [45]. The presence of the broad peak at 20.533 °θ in AG-PVP indicates the great miscibility and complexation between the two polymers. In the XRD pattern of AG-PVP-HAp, a peak at 32.2 °θ was detected. In the XRD pattern for the standard hydroxyapatite phase (JCPDS card no. 09-432), this peak (32.2 °θ) is a sharp peak, while in the spectrum of the AG-PVP-HAp the intensity ratio of this peak is reduced. Thus, the presence of this peak confirms the addition of HAp to the composite and its reduced intensity ratio shows complexation with the amorphous structure of AG-PVP. Also, the intensity ratio of the broad peak detected in the AG-PVP pattern has decreased in the AG-PVP-HAp pattern and indicates the formation of an amorphous structure. As reported in the literature, quercetin has a crystalline structure with characteristic diffraction peaks [35]. The successful incorporation of QC in the amorphous nanocomposite is observed since the XRD pattern of AG-PVP-HAp-QC exhibits none of the crystalline peaks of QC as a result of complexation with other components of the fabricated nanocomposite. In addition, the FTIR results proved the presence of QC in the nanocomposite.

3.1.3. Morphology observation

Morphology observation of freeze-dried hydrogel nanocomposites loaded with quercetin was performed via FESEM (Fig. 6). From the images, it is evident that most of the nanocomposites have a spherical shape with a solid, dense structure. The best shape of nanoparticles in drug delivery application is spherical shape [46]. Good compatibility between nanocomposite components was evident from the homogeneous surface of the nanocomposite. Polydispersity and size of nanocarriers were determined using DLS analysis. The nanocarriers' particle size distribution ranged from 440 nm to 536 nm, with a PDI index of 0.4. As reported in the literature, this value for polydispersity is acceptable for drug delivery applications [47].

Besides, the zeta potential values can confirm the stability of nanocarriers. In this regard, the Zeta potential values of the nanocarriers were between -28.1 to -29.5 mV confirming the nanocarriers' good stability[48].

3.2. HAp nanoparticles impact on quercetin loading and entrapment efficiency

As stated before, one of the main challenges for the application of QC is its poor solubility (2 μg mL^{-1}), which results in its low bioavailability [49,50]. Thus, ameliorating the loading efficiency of QC is a challenge. In this study, the loading and encapsulation efficiencies of AG-PVP-QC and AG-PVP-HAp-QC were measured using equations Eq_1 and Eq_2, respectively, to investigate the impact of HAp nanoparticles on these parameters. The loading efficiency for QC-loaded AG-PVP hydrogel without HAp was 48 %. This efficiency increased to 61 % in AG-PVP-HAp-QC. This increase is attributed to the contribution of HAp nanoparticles to enhanced loading capacity in the AG-PVP hydrogel. Indeed, the bonding between components like hydrogen bonding between the carbonyl group of PVP and hydroxyl groups of AG, HAp, and QC leads to forming a high interpenetrating biopolymeric network. This interlocked structure of the crosslinked interpenetrating polymer network results in entrapment of the model drug in the structure and improves the loading capacity [51]. The change in the FTIR spectrum when quercetin combined with the hydrogel containing HAp nanoparticles confirmed these interplays between drug and nanocomposites. Furthermore, the introduction of HAp into AG-PVP hydrogel affords more surface interactions between polymers, HAp, and the drug due to the high surface area of HAp nanoparticles.

The achieved loading was higher than other pH-responsive systems developed so far. For instance, Rahimi et al. developed rod-like chitosan–quinoline nanoparticles as pH-responsive nanocarriers with 9.6 % drug loading efficiency [52]. Tiwari et al. synthesized functionalized graphene oxide (GO)- polyvinylpyrrolidone (PVP) for dual delivery of quercetin and gefitinib to ovarian cancer cells. In this developed dual delivery system, 20 % of quercetin and 46 % of gefitinib were loaded on GO-PVP nanocarrier [53]. In a study to formulate quercetin within liposomes for skin delivery, the drug loading efficiency was 2.58% [7]. Kumar et al. prepared solid lipid nanoparticles (SLN) and nano lipidic carriers (NLC) with a loading efficiency of 16.65 % and 17.98 %, respectively [54]. The attained drug loading in this study shows a drastic increase compared to previous studies [55,56].

Also, the encapsulation efficiency of quercetin was 85 % in AG-PVP hydrogel and 93 % in AG-PVP-HAp hydrogel nanocomposite, which proved the high affinity of QC to the nanocomposite owing to the same reason discussed above. Likewise, the encapsulation efficiency in this study was higher than reported efficiencies like quercetin encapsulation efficiency in rod-like chitosan–quinoline nanoparticles [52], quercetin entrapped in quantum dots [57], solid lipid nanoparticles, and nano lipid carriers [54]. The drug loading and encapsulation efficiencies in AG-PVP and AG-PVP-HAp with the percentage of the increase due to the addition of HAp nanoparticles are summarized in Table. 1. Moreover, in Table. 2, the encapsulation and loading efficiencies reported in former studies and the current study are summarized.

3.3. Release of quercetin from the nanocarriers

The objective of analyzing the release behavior was to affirm the fabricated platform's pH-responsive and sustained-release behavior. For this purpose, the release of QC from nanocarriers was examined by the dialysis method as mentioned before at two different buffer mediums (pH 7.4 and 5.4) at 37 °C (the normal temperature of the human body), throughout 96 h (Fig. 7). As

can be seen, the cumulative release of QC from nanoemulsions containing AG-PVP-HAp, and AG-PVP at pH 7.4 after 24 h was 28% and 33%, respectively. On the other hand, the cumulative release after 24 h at pH 5.4 (acidic media) reached 54 % for AG-PVP-HAp and 40% for AG-PVP, respectively. The cumulative release from AG-PVP-HAp at pH 7.4 is less than AG-PVP due to the effect of HAp nanoparticles. Indeed, the interactions between nanoparticles, polymers, and the model drug maintain the integrity of the nanocomposite structure, which leads to a decrease in cumulative release for AG-PVP-HAp-QC compared to AG-PVP-QC at pH=7.4. After 96 h, 93.5 % of quercetin was released at pH 5.4, while only 76 % of quercetin was released at pH 7.4. Besides, a primary gradual release preceded the sustained release of quercetin at pH 7.4 as it can be seen in Fig. 7.

This slow-release and retention behavior at basic conditions retains the drug when the nanocarrier passes to reach the tumor cells to release the drug at the target site. The difference in the release behavior at pH 5.4 and 7.4 for the groups containing HAp demonstrates the pH-responsive behavior of the fabricated nanocarrier. This property is ascribed to the accelerated dissolution of HAp (calcium phosphate) at acidic conditions due to the protonation of HAp. This protonation along with the protonation of carbonyl groups in PVP, hydroxyl groups in QC and AG leads to a repulsive force between the adjacent positive charge in Ca^{2+} (HAp) and other protonated groups, which intensifies the repulsive force and facilitates the dissolution of the nanocomposite, thereby increasing the amount of drug released. Thus, an increase in drug release rates for AG-PVP-HAp-QC at pH 5.4 could be allocated to the pH sensitivity of HAp and protonation of polymers at low pH [32]. The statistical analysis performed between groups showed significant difference between pH 5.4 with HAp as control group and all other groups with $p< 0.001$. The values of QC cumulative release percentage in each time point for all groups are shown in Fig. 10. The significant difference between pH 5.4 with HAp and all other groups at all time points is also shown in Fig. 8.

Also, the release profile of QC from AG-PVP-HAp hydrogel not encapsulated in double emulsions at pH=5.4 represents the effect of the double emulsion on the sustained release compared to the group encapsulated in the double emulsion at pH=5.4. As can be seen, more than 80 % of the drug was released at acidic condition after 24 h. This amount decreased to 54 % for the group incorporated in the double emulsion. This is due to the effect of the intermediate oil layer in water in oil in water double emulsion. After the dissolution of the nanocomposite, this layer acts as a membrane to control the release of QC and prolongs the release period. Moreover, the presence of PVA as a surfactant in the aqueous phase of the secondary emulsion further stabilizes the nanocarrier and prolongs the release period. The same result was observed in a nanocarrier of Chitosan-carbon quantum dot- aptamer complex [36]. Therefore, the double emulsion prolongs the release from the fabricated pH-sensitive hydrogel at acidic conditions. The effect of double emulsions on prolonging the release time can be seen by comparing the release behavior of quercetin-loaded chitosan-cellulose hydrogel with zinc oxide nanoparticles fabricated by George et al [58]. The fabricated platform was pH-responsive owing to the pH-sensitivity of chitosan [59]. At acidic condition (pH 5), approximately 40 % of quercetin was released during one hour, whereas in this study, 40 % of QC was released during 12 h at pH 5.4, which shows the sustained-release of QC. Also, calcium phosphate nanocomposites developed by Patra et al. showed 57 % drug release within the first 8 h [60], whereas in the current study,

57 % of the drug was released in more than 24 hours.

3.4. Kinetic modeling of drug release

The drug release kinetics was evaluated using the drug release data acquired through the dialysis method [37]. The release data at neutral and acidic pH were fitted to zero-order, first-order, Higuchi model, Hixson-Crowell model, and Korsmeyer-Peppas model to determine the release mechanism for each pH. Fitting the release data to the mentioned models showed that based on the R square values of the models with only meaningful parameters, the release data best fit the Korsmeyer-Peppas model with a higher R^2 value at pH 7.4. The parameters of regressions were tested by p-value< 0.05, and as stated parameters without a meaningful effect on the models were omitted.

The Korsmeyer–Peppas model is applied to analyze the release of the drug from the dosage form, mainly when the release mechanism is complex and involves more than one type. In this model, n is the diffusional exponent representing the mechanism of drug release. For pH 7.4, the n value for this model was 0.6044. According to the classifications for this model, the release mechanism is anomalous transport [61,62]. In addition, the exponent n in the range 0.43-0.59 corresponds to a primarily diffusion-controlled release mechanism [63]. This release mechanism is aligned with the structure of the fabricated nanocarrier and the interactions between the components. Indeed, the physical and chemical interactions between the drug and components maintain nanocarrier's integrity and prevents the dissolution of the nanocarrier at neutral conditions. Hence, the release mechanism at neutral condition is mainly based on diffusion. The same result was reported by Zhao et al. in preparing a composite hydrogel as the carrier of apigenin [64].

Also, the release data at pH 5.4 were fitted to the mentioned models. The R^2 values of the fitted models showed the Korsmeyer-Peppas model fitted better than other models to release data (Fig. 9). The n value of the Korsmeyer-Peppas model was 0.8155 at pH=5.4. According to the Korsmeyer-Peppas model for n values between 0.43 and 0.85 the mechanism of release is anomalous transport (non-fickian). At this pH, the increase of the n value from 0.6044 to 0.8155 denotes transition of the principal release mechanism from diffusion to dissolution. This change in the major release mechanism is due to the accelerated dissolution of HAp in acidic condition which releases positive charge in Ca^{2+} (HAp). Also, the protonation of other mentioned functional groups in the nanocomposite produces a repulsive force between the adjacent positive charges and accelerates the dissolution of the nanocomposite. Therefore, at acidic condition, the dissolution occurs faster than diffusion.

In addition, other kinetic models regressed from the release date confirm the results described above. For instance, zero order model does not fit both conditions since in this model release is independent of concentration. The release date fit first-order model better, which shows the release is concentration dependent [65]. Besides, the Higuchi model is used for the release of a drug from a dosage which involves both diffusion and dissolution. The release data at pH 7.4 and 5.4 fit this model with R square 0.9824 and 0.9871, respectively. The good fitting of the release data to this model represents the occurrence of diffusion and dissolution during release, which is in accord with the results from the Korsmeyer-Peppas model. Furthermore, the Hixson-Crowell model, which is used for dissolution-controlled release, is fitted better with the release data at pH 5.4 and confirms dissolution is more dominant in release at pH 5.4 due to the increased repulsive forces between components after protonation at acidic pH [65]. Accordingly, the release mechanism is anomalous according to the Korsmeyer-Peppas model as the best fitting

model with transition from diffusion to dissolution as predominant mechanism at pH 7.4 and 5.4, respectively.

Drug release data fitted to mathematical models of drug release are represented in Fig. 9. The results of kinetic modeling of the drug release are also summarized in Table. 3.

3.5. In-vitro cytotoxicity study

MTT analysis was conducted to assess the cytotoxicity of the prepared QC-loaded nanocarriers to examine whether the prepared nanocarriers can be adopted for the delivery of QC with significant growth inhibitory effects compared to free QC. The cytotoxic effects of free QC, nanocarriers of AG-PVP-QC, AG-PVP-HAp-QC on MCF-7 cells after 72 h incubation were evaluated using the MTT assay presented in Fig. 10. Also, the viability of cells treated with AG-PVP-HAp was studied to evaluate the nanocarrier's cytotoxicity. According to the literature, hydrogels of PVP and agarose have not shown significant cytotoxic effects even at higher concentrations of this study [66,67]. Therefore, the observed decrease in the viability of cells in AG-PVP-HAp sample accounts for the in vitro cytotoxicity of HAp. A similar reduction in the viability percentage is reported for the cytotoxicity of HAp on MCF-7 cells with a concentration equal to the concentration in this study. [68,69]. Therefore, the reduction in the viability of control cells with $p< 0.01$ confirmed the in vitro cytotoxicity of HAp. Besides, the viability of cells treated with free QC is less than AG-PVP-HAp group with $p< 0.01$, which shows QC with applied concentration has more cytotoxic effect on the cells than HAp. The reduction in the viability of cells treated with free QC is consistent with the results of former studies in the literature [70].

The viability of cells treated with free QC is less than cells treated with AG-PVP-QC with $p< 0.05$. This could be due to the fact that QC is a hydrophobic drug and is expected to have direct interaction with cells through penetration into lipid membranes without fulfilling the release process from AG-PVP nanocarrier. Moreover, the viability of cells treated with the fabricated nanocarrier of AG-PVP-HAp-QC is less than free QC and AG-PVP-QC with $p< 0.001$. This result represents significant cytotoxicity of AG-PVP-HAp-QC on cancer cells based on the antiproliferative effect of HAp nanoparticles along with anticancer activity of QC as well as improved release behavior of the nanocarrier. Indeed, the enhanced sustained-release of QC from AG-PVP-HAp-QC due to HAp nanoparticles and nanoemulsions leads to the sustained and time-dependent release of QC, which reduces viability through improving apoptosis induction on the cells. Flow cytometry assay was performed to study the cytotoxicity of the carrier further and verify this explanation.

3.6. Cell apoptosis assay

To further analyze the biological property of the prepared nanocarrier and figure out the impact of sustained-release due to the use of HAp and double emulsions on improved QC cytotoxicity, cell apoptosis assay was used to study the apoptotic and necrotic induction effect of QC loaded in AG-PVP, AG-PVP-HAp, free QC, and blank AG-PVP-HAp (without drug loading). The reduction in the percentage of Q4, denoting viable cells, in blank AG-PVP-HAp compared to the control group was less than other groups. This result is aligned with the MTT results discussed before. Besides, the percentage of apoptotic cells in AG-PVP-HAp increased compared to the control group. This result represents the apoptosis induction feature of HAp reported in the literature [71]. According to Fig. 11, the percentage of viable cells in free QC is

less than AG-PVP-QC, which is again in agreement with the cytotoxicity results. Also, as mentioned before, since cells have been directly exposed to free QC, the percentage of necrotic cells in free QC (51.8%) is higher than AG-PVP-QC. This reduction in the percentage of necrotic cells in AG-PVP-QC can be attributed to nanoemulsions for incorporating AG-PVP-QC that has gradually released QC compared to free QC and led to less necrosis. Thus, the higher cytotoxicity of free QC than AG-PVP-QC observed in the MTT results is mainly due to necrosis. The percentage of early and late apoptotic cells in AG-PVP-HAp-QC is higher than other samples with the lowest percentage of viable cells (6.55%). This result represents the improved cytotoxicity of QC through further apoptosis induction by the sustained release owing to the use of nanoparticles and double emulsion along with the apoptotic effects of nanoparticles.

Besides, the percentage of necrotic cells in AG-PVP-HAp-QC reduced compared to free quercetin, which shows the majority of cells are in the early or late apoptotic phase, while in free QC most of the cells are in the necrotic phase (Q1). The same result was observed in the study gold nanoparticles-conjugated quercetin on apoptosis induction in MCF-7 cells. Gold nanoparticles-QC treated cells had more early and late apoptotic cells than free QC treated cells [72]. The achieved value of apoptosis by quercetin-loaded AG-PVP-HAp is much higher than the cotreatment of MCF-7 cells with rhTRAIL and quercetin reported to be 25% [73]. Therefore, the enhanced apoptosis induction of QC can be attributed to the improved sustained-release behavior of the fabricated nanocarrier by the interaction between HAp nanoparticles with anticancer activity and the drug as well as the role of double emulsion that released QC gradually and induced apoptosis in more cells with time. Consequently, this system provided a considerable antitumor effect.

4. Conclusion

Despite the promising features of quercetin as an anticancer drug, its targeted delivery over a period of time is a challenge due to poor solubility and short biological half-life time. Thus, developing a platform with stimuli-responsive property for targeted delivery, enhancing its loading, and extending the release time is necessary. In this work, a pH-responsive nanocomposite encapsulated in nanoemulsions was developed to simultaneously enhance the loading and sustained-release of quercetin with the use of HAp nanoparticles and nanoemulsions. In conclusion, incorporating HAp nanoparticles into nanocomposites ameliorates the loading efficiency and provides pH-responsive release behavior. The use of nanoparticles controls the drug's burst release due to its interactions with the drug and polymers in the nanocomposite structure to retain the drug at pH 7.4 and release it at the tumor site with lower pH. Also, the incorporation of nanocomposites in nanoemulsions prolonged the release time further by the oil layer of W/O/W emulsion, acting as a membrane to control the release of QC. Besides, the prepared nanocarriers with this approach significantly enhanced the apoptosis induction activity of QC compared to free QC or QC-loaded AG-PVP hydrogel. Hence, the prepared nanocarrier can be used as a potential pH-sensitive nanocarrier for the controlled release of quercetin to address the mentioned defects attributed to QC as an anticancer drug.

5. References

[1] Q. Wu, P.W. Needs, Y. Lu, P.A. Kroon, D. Ren, X. Yang, Different antitumor effects of quercetin, quercetin-3′-sulfate and quercetin-3-glucuronide in human breast cancer MCF-7 cells, Food Funct. 9 (2018) 1736–1746. https://doi.org/10.1039/c7fo01964e.

[2] A.G. Sauer, A. Jemal, R.L. Siegel, K.D. Miller, Breast Cancer Statistics , 2019, 0 (2019) 1–14. https://doi.org/10.3322/caac.21583.
[3] and S.P. Alexander Victor Anand David, Radhakrishnan Arulmoli, Overviews of Biological Importance of Quercetin: A Bioactive Flavonoid, Pharmacogn Rev. 10 (n.d.) 84–89.
[4] H. Wu, Y. Zhao, X. Mu, H. Wu, Journal of Biomaterials Science , A silica – polymer composite nano system for tumor-targeted imaging and p53 gene therapy of lung cancer, (2015) 37–41. https://doi.org/10.1080/09205063.2015.1012035.
[5] R. Penalva, C.J. González-Navarro, C. Gamazo, I. Esparza, J.M. Irache, Zein nanoparticles for oral delivery of quercetin: Pharmacokinetic studies and preventive anti-inflammatory effects in a mouse model of endotoxemia, Nanomedicine Nanotechnology, Biol. Med. 13 (2017) 103–110. https://doi.org/10.1016/j.nano.2016.08.033.
[6] B. Lu, Y. Huang, Z. Chen, J. Ye, H. Xu, W. Chen, X. Long, Liposomal nanocarriers for enhanced skin delivery of quercetin with functions of anti-tyrosinase and antioxidant, Molecules. 24 (2019). https://doi.org/10.3390/molecules24122322.
[7] T. Hatahet, M. Morille, A. Hommoss, J.M. Devoissellc, R. H. Müller, S. Bégu, Liposomes, lipid nanocapsules and smartCrystals®: A comparative study for an effective quercetin delivery to the skin, Int. J. Pharm. 542 (2018) 176–185. https://doi.org/10.1016/j.ijpharm.2018.03.019.
[8] V. García-Mediavilla, I. Crespo, P.S. Collado, A. Esteller, S. Sánchez-Campos, M.J. Tuñón, J. González-Gallego, The anti-inflammatory flavones quercetin and kaempferol cause inhibition of inducible nitric oxide synthase, cyclooxygenase-2 and reactive C-protein, and down-regulation of the nuclear factor kappaB pathway in Chang Liver cells, Eur. J. Pharmacol. 557 (2007) 221–229. https://doi.org/10.1016/j.ejphar.2006.11.014.
[9] L. Jia, S. Huang, X. Yin, Y. Zan, Y. Guo, L. Han, Quercetin suppresses the mobility of breast cancer by suppressing glycolysis through Akt-mTOR pathway mediated autophagy induction, Life Sci. 208 (2018) 123–130. https://doi.org/10.1016/j.lfs.2018.07.027.
[10] G. Scambia, F.O. Ranelletti, P.B. Panici, R. De Vincenzo, G. Bonanno, G. Ferrandina, M. Piantelli, S. Bussa, C. Rumi, M. Cianfriglia, S. Mancuso, Quercetin potentiates the effect of adriamycin in a multidrug-resistant MCF-7 human breast-cancer cell line: P-glycoprotein as a possible target, Cancer Chemother. Pharmacol. 34 (1994) 459–464. https://doi.org/10.1007/BF00685655.
[11] M. Hemati, F. Haghiralsadat, F. Yazdian, F. Jafari, A. Moradi, Z. Malekpour-Dehkordi, Development and characterization of a novel cationic PEGylated niosome-encapsulated forms of doxorubicin, quercetin and siRNA for the treatment of cancer by using combination therapy, Artif. Cells, Nanomedicine Biotechnol. 47 (2019) 1295–1311. https://doi.org/10.1080/21691401.2018.1489271.
[12] A. Sarkar, S. Ghosh, S. Chowdhury, B. Pandey, P.C. Sil, Targeted delivery of quercetin loaded mesoporous silica nanoparticles to the breast cancer cells, Biochim. Biophys. Acta - Gen. Subj. 1860 (2016) 2065–2075. https://doi.org/10.1016/j.bbagen.2016.07.001.
[13] A. Maghsoudi, F. Yazdian, S. Shahmoradi, L. Ghaderi, M. Hemati, G. Amoabediny, Curcumin-loaded polysaccharide nanoparticles: Optimization and anticariogenic activity against Streptococcus mutans, Mater. Sci. Eng. C. 75 (2017) 1259–1267. https://doi.org/10.1016/j.msec.2017.03.032.
[14] R. Awasthi, S. Manchanda, P. Das, V. Velu, H. Malipeddi, K. Pabreja, T.D.J.A. Pinto, G. Gupta, K. Dua, Poly(vinylpyrrolidone)- Chapter 9, in: Eng. Biomater. Drug Deliv. Syst.

Beyond Polyethyl. Glycol, Elsevier Ltd, 2018: pp. 255–272. https://doi.org/10.1016/B978-0-08-101750-0.00009-X.

[15] P. Priya, A. Raja, V. Raj, Interpenetrating polymeric networks of chitosan and egg white with dual crosslinking agents polyethylene glycol/polyvinylpyrrolidone as a novel drug carrier, Cellulose. 23 (2016) 699–712. https://doi.org/10.1007/s10570-015-0821-x.

[16] L. Cao, X. Wu, Q. Wang, J. Wang, Biocompatible nanocomposite of TiO2 incorporated bi-polymer for articular cartilage tissue regeneration: A facile material, J. Photochem. Photobiol. B Biol. 178 (2018) 440–446. https://doi.org/10.1016/j.jphotobiol.2017.10.026.

[17] X. Qi, T. Su, X. Tong, W. Xiong, Q. Zeng, Y. Qian, Z. Zhou, X. Wu, Z. Li, L. Shen, X. He, C. Xu, M. Chen, Y. Li, J. Shen, Facile formation of salecan/agarose hydrogels with tunable structural properties for cell culture, Carbohydr. Polym. 224 (2019) 115208. https://doi.org/10.1016/j.carbpol.2019.115208.

[18] N. Ninan, A. Forget, V.P. Shastri, N.H. Voelcker, A. Blencowe, Antibacterial and Anti-Inflammatory pH-Responsive Tannic Acid-Carboxylated Agarose Composite Hydrogels for Wound Healing, ACS Appl. Mater. Interfaces. 8 (2016) 28511–28521. https://doi.org/10.1021/acsami.6b10491.

[19] M. van Elk, B.P. Murphy, T. Eufrásio-da-Silva, D.P. O'Reilly, T. Vermonden, P.W.E. Hennink, G.P. Duffy, E. Ruiz-Hernández, Nanomedicines for advanced cancer treatments: Transitioning towards responsive systems, Int. J. Pharm. 515 (2016) 132–164. https://doi.org/10.1016/j.ijpharm.2016.10.013.

[20] N. Malekimusavi, H., Ghaemi, A., Masoudi, G., Chogan, F., Rashedi, H., Yazdian, F., Omidi, M., Javadi, S., Haghiralsadat, B.F., Teimouri, M. and Faal Hamedani, Graphene oxide-l-arginine nanogel A pH-sensitive fluorouracil nanocarrier, Biotechnol. Appl. Biochem. 66 (2019) pp.772-780. https://doi.org/10.1002/bab.1768.

[21] P. Date, A. Tanwar, P. Ladage, K.M. Kodam, D. Ottoor, Carbon dots-incorporated pH-responsive agarose-PVA hydrogel nanocomposites for the controlled release of norfloxacin drug, Polym. Bull. 77 (2020) 5323–5344. https://doi.org/10.1007/s00289-019-03015-3.

[22] K. Wang, H.F. Wen, D.G. Yu, Y. Yang, D.F. Zhang, Electrosprayed hydrophilic nanocomposites coated with shellac for colon-specific delayed drug delivery, Mater. Des. 143 (2018) 248–255. https://doi.org/10.1016/j.matdes.2018.02.016.

[23] Y. Ding, C. Dou, S. Chang, Z. Xie, D.G. Yu, Y. Liu, J. Shao, Core-shell eudragit S100 nanofibers prepared via triaxial electrospinning to providea colon-targeted extended drug release, Polymers (Basel). 12 (2020). https://doi.org/10.3390/POLYM12092034.

[24] E. Larrañeta, S. Stewart, M. Ervine, R. Al-Kasasbeh, R.F. Donnelly, Hydrogels for hydrophobic drug delivery. Classification, synthesis and applications, J. Funct. Biomater. 9 (2018). https://doi.org/10.3390/jfb9010013.

[25] D.F. Argenta, T.C. dos Santos, A.M. Campos, T. Caon, Hydrogel Nanocomposite Systems- Chapter 3, in: Nanocarriers Drug Deliv. Nanosci. Nanotechnol. Drug Deliv., 2019: pp. 81–131. https://doi.org/10.1016/b978-0-12-814033-8.00003-5.

[26] L. Kong, Z. Mu, Y. Yu, L. Zhang, J. Hu, Polyethyleneimine-stabilized hydroxyapatite nanoparticles modified with hyaluronic acid for targeted drug delivery, RSC Adv. 6 (2016) 101790–101799. https://doi.org/10.1039/c6ra19351j.

[27] L. Fan, J. Zhang, A. Wang, In situ generation of sodium alginate/hydroxyapatite/halloysite nanotubes nanocomposite hydrogel beads as drug-controlled release matrices, J. Mater. Chem. B. 1 (2013) 6261–6270. https://doi.org/10.1039/c3tb20971g.

[28] H. Zhao, C. Wu, D. Gao, S. Chen, Y. Zhu, J. Sun, H. Luo, K. Yu, H. Fan, X. Zhang, Antitumor effect by hydroxyapatite nanospheres: Activation of mitochondria-dependent apoptosis and negative regulation of phosphatidylinositol-3-kinase/protein kinase B pathway, ACS Nano. 12 (2018) 7838–7854. https://doi.org/10.1021/acsnano.8b01996.

[29] A.T.& P.J.S. A RAWAT, H K MAHAVAR, Study of electrical properties of polyvinylpyrrolidone/polyacrylamide blend thin films, Bull. Mater. Sci. 37 (2014) 273–279.

[30] P. Zucca, R. Fernandez-Lafuente, E. Sanjust, Agarose and its derivatives as supports for enzyme immobilization, Molecules. 21 (2016) 1–25. https://doi.org/10.3390/molecules21111577.

[31] Y. Ryabenkova, N. Jadav, M. Conte, M.F.A. Hippler, N. Reeves-Mclaren, P.D. Coates, P. Twigg, A. Paradkar, Mechanism of Hydrogen-Bonded Complex Formation between Ibuprofen and Nanocrystalline Hydroxyapatite, Langmuir. 33 (2017) 2965–2976. https://doi.org/10.1021/acs.langmuir.6b04510.

[32] M. Lelli, N. Roveri, C. Marzano, J.D. Hoeschele, A. Curci, N. Margiotta, V. Gandin, G. Natile, Hydroxyapatite nanocrystals as a smart, pH sensitive, delivery system for kiteplatin, Dalt. Trans. 45 (2016) 13187–13195. https://doi.org/10.1039/c6dt01976e.

[33] M. Chouaibi, J. Mejri, L. Rezig, K. Abdelli, S. Hamdi, Experimental study of quercetin microencapsulation using water-in-oil-in-water (W1/O/W2) double emulsion, Elsevier B.V, 2019. https://doi.org/10.1016/j.molliq.2018.10.030.

[34] T.K. Giri, C. Choudhary, Ajazuddin, A. Alexander, H. Badwaik, D.K. Tripathi, Prospects of pharmaceuticals and biopharmaceuticals loaded microparticles prepared by double emulsion technique for controlled delivery, Saudi Pharm. J. 21 (2013) 125–141. https://doi.org/10.1016/j.jsps.2012.05.009.

[35] Z. Aytac, S.I. Kusku, E. Durgun, T. Uyar, Quercetin/β-cyclodextrin inclusion complex embedded nanofibres: Slow release and high solubility, Food Chem. 197 (2016) 864–871. https://doi.org/10.1016/j.foodchem.2015.11.051.

[36] H.S. Zavareh, M. Pourmadadi, A. Moradi, F. Yazdian, M. Omidi, Chitosan/carbon quantum dot/aptamer complex as a potential anticancer drug delivery system towards the release of 5-fluorouracil, Int. J. Biol. Macromol. (2020). https://doi.org/10.1016/j.ijbiomac.2020.09.166.

[37] B.R. Shah, Y. Li, W. Jin, Y. An, L. He, Z. Li, W. Xu, B. Li, Preparation and optimization of Pickering emulsion stabilized by chitosan-tripolyphosphate nanoparticles for curcumin encapsulation, Food Hydrocoll. 52 (2016) 369–377. https://doi.org/10.1016/j.foodhyd.2015.07.015.

[38] G.P. Kumar, A.R. Phani, R.G.S.V. Prasad, J.S. Sanganal, N. Manali, R. Gupta, N. Rashmi, G.S. Prabhakara, C.P. Salins, K. Sandeep, D.B. Raju, Polyvinylpyrrolidone oral films of enrofloxacin: Film characterization and drug release, Int. J. Pharm. 471 (2014) 146–152. https://doi.org/10.1016/j.ijpharm.2014.05.033.

[39] Z. Zhang, X. Zhang, Z. Xin, M. Deng, Y. Wen, Y. Song, Synthesis of monodisperse silver nanoparticles for ink-jet printed flexible electronics, Nanotechnology. 22 (2011). https://doi.org/10.1088/0957-4484/22/42/425601.

[40] F. Wang, W. Xiao, M.A. Elbahnasawy, X. Bao, Q. Zheng, L. Gong, Y. Zhou, S. Yang, A. Fang, M.M.S. Farag, J. Wu, X. Song, Optimization of the linker length of mannose-cholesterol conjugates for enhanced mRNA delivery to dendritic cells by liposomes, Front. Pharmacol. 9 (2018) 1–14. https://doi.org/10.3389/fphar.2018.00980.

[41] B. Samiey, F. Ashoori, Adsorptive removal of methylene blue by agar: Effects of NaCl and ethanol, Chem. Cent. J. 6 (2012) 14. https://doi.org/10.1186/1752-153X-6-14.
[42] C.Y. Ooi, M. Hamdi, S. Ramesh, Properties of hydroxyapatite produced by annealing of bovine bone, Ceram. Int. 33 (2007) 1171–1177. https://doi.org/10.1016/j.ceramint.2006.04.001.
[43] B. Pawlikowska-Pawlęga, H. Dziubińska, E. Król, K. Trębacz, A. Jarosz-Wilkołazka, R. Paduch, A. Gawron, W.I. Gruszecki, Characteristics of quercetin interactions with liposomal and vacuolar membranes, Biochim. Biophys. Acta - Biomembr. 1838 (2014) 254–265. https://doi.org/10.1016/j.bbamem.2013.08.014.
[44] B. MAQ, M.S. Rahman, Improvement of Swelling Behaviour of Poly (Vinyl Pyrrolidone) and Acrylic Acid Blend Hydrogel Prepared By the Application of Gamma Radiation, Org. Chem. Curr. Res. 04 (2015). https://doi.org/10.4172/2161-0401.1000138.
[45] R. Singh, N.A. Jadhav, S. Majumder, B. Bhattacharya, P.K. Singh, Novel biopolymer gel electrolyte for dye-sensitized solar cell application, Carbohydr. Polym. 91 (2013) 682–685. https://doi.org/10.1016/j.carbpol.2012.08.055.
[46] G. Prabha, V. Raj, Preparation and characterization of chitosan - Polyethylene glycol-polyvinylpyrrolidone-coated superparamagnetic iron oxide nanoparticles as carrier system: Drug loading and in vitro drug release study, J. Biomed. Mater. Res. - Part B Appl. Biomater. 104 (2016) 808–816. https://doi.org/10.1002/jbm.b.33637.
[47] A. Sedaghat Doost, V. Kassozi, C. Grootaert, M. Claeys, K. Dewettinck, J. Van Camp, P. Van der Meeren, Self-assembly, functionality, and in-vitro properties of quercetin loaded nanoparticles based on shellac-almond gum biological macromolecules, Int. J. Biol. Macromol. 129 (2019) 1024–1033. https://doi.org/10.1016/j.ijbiomac.2019.02.071.
[48] E. Joseph, G. Singhvi, Multifunctional nanocrystals for cancer therapy: A potential nanocarrier, in: Nanomater. Drug Deliv. Ther., Elsevier Inc., 2019: pp. 91–116. https://doi.org/10.1016/B978-0-12-816505-8.00007-2.
[49] F. Sheng, P.S. Chow, J. Hu, S. Cheng, L. Guo, Y. Dong, Preparation of quercetin nanorod/microcrystalline cellulose formulation via fluid bed coating crystallization for dissolution enhancement, Int. J. Pharm. 576 (2020) 118983. https://doi.org/10.1016/j.ijpharm.2019.118983.
[50] M. Imran, M.K. Iqubal, K. Imtiyaz, S. Saleem, S. Mittal, M.M.A. Rizvi, J. Ali, S. Baboota, Topical nanostructured lipid carrier gel of quercetin and resveratrol: Formulation, optimization, in vitro and ex vivo study for the treatment of skin cancer, Int. J. Pharm. 587 (2020) 119705. https://doi.org/10.1016/j.ijpharm.2020.119705.
[51] D. Kumarasamy, T.K. Giri, Biopolysaccharide-based hydrogel materials for drug delivery, in: Polysacch. Carriers Drug Deliv., Elsevier Ltd., 2019: pp. 585–613. https://doi.org/10.1016/B978-0-08-102553-6.00020-9.
[52] S. Rahimi, S. Khoee, M. Ghandi, Preparation and characterization of rod-like chitosan–quinoline nanoparticles as pH-responsive nanocarriers for quercetin delivery, Int. J. Biol. Macromol. 128 (2019) 279–289. https://doi.org/10.1016/j.ijbiomac.2019.01.137.
[53] H. Tiwari, N. Karki, M. Pal, S. Basak, R.K. Verma, R. Bal, N.D. Kandpal, G. Bisht, N.G. Sahoo, Functionalized graphene oxide as a nanocarrier for dual drug delivery applications: The synergistic effect of quercetin and gefitinib against ovarian cancer cells, Colloids Surfaces B Biointerfaces. 178 (2019) 452–459. https://doi.org/10.1016/j.colsurfb.2019.03.037.
[54] P. Kumar, G. Sharma, R. Kumar, B. Singh, R. Malik, O.P. Katare, K. Raza, Promises of a

biocompatible nanocarrier in improved brain delivery of quercetin: Biochemical, pharmacokinetic and biodistribution evidences, Int. J. Pharm. 515 (2016) 307–314. https://doi.org/10.1016/j.ijpharm.2016.10.024.

[55] L. Liu, Y. Tang, C. Gao, Y. Li, S. Chen, T. Xiong, J. Li, M. Du, Z. Gong, H. Chen, P. Yao, Characterization and biodistribution in vivo of quercetin-loaded cationic nanostructured lipid carriers, Colloids Surfaces B Biointerfaces. 115 (2014) 125–131. https://doi.org/10.1016/j.colsurfb.2013.11.029.

[56] S. Rajesh Kumar, S. Priyatharshni, V.N. Babu, D. Mangalaraj, C. Viswanathan, S. Kannan, N. Ponpandian, Quercetin conjugated superparamagnetic magnetite nanoparticles for in-vitro analysis of breast cancer cell lines for chemotherapy applications, J. Colloid Interface Sci. 436 (2014) 234–242. https://doi.org/10.1016/j.jcis.2014.08.064.

[57] R. Jeyadevi, T. Sivasudha, A. Rameshkumar, D.A. Ananth, G.S.B. Aseervatham, K. Kumaresan, L.D. Kumar, S. Jagadeeswari, R. Renganathan, Enhancement of anti arthritic effect of quercetin using thioglycolic acid-capped cadmium telluride quantum dots as nanocarrier in adjuvant induced arthritic Wistar rats, Colloids Surfaces B Biointerfaces. 112 (2013) 255–263. https://doi.org/10.1016/j.colsurfb.2013.07.065.

[58] D. George, P.U. Maheswari, K.M.M.S. Begum, Synergic formulation of onion peel quercetin loaded chitosan-cellulose hydrogel with green zinc oxide nanoparticles towards controlled release, biocompatibility, antimicrobial and anticancer activity, Int. J. Biol. Macromol. 132 (2019) 784–794. https://doi.org/10.1016/j.ijbiomac.2019.04.008.

[59] E. Marsano, E. Bianchi, S. Vicini, L. Compagnino, A. Sionkowska, J. Skopińska, M. Wiśniewski, Stimuli responsive gels based on interpenetrating network of chitosan and poly(vinylpyrrolidone), Polymer (Guildf). 46 (2005) 1595–1600. https://doi.org/10.1016/j.polymer.2004.12.017.

[60] M. Patra, R. Mukherjee, M. Banik, D. Dutta, N.A. Begum, T. Basu, Calcium phosphate-quercetin nanocomposite (CPQN): A multi-functional nanoparticle having pH indicating, highly fluorescent and anti-oxidant properties, Colloids Surfaces B Biointerfaces. 154 (2017) 63–73. https://doi.org/10.1016/j.colsurfb.2017.03.018.

[61] M.L. Bruschi, Mathematical models of drug release, Strateg. to Modify Drug Release from Pharm. Syst. (2015) 63–86. https://doi.org/10.1016/b978-0-08-100092-2.00005-9.

[62] R.W. Korsmeyer, R. Gurny, E. Doelker, P. Buri, N.A. Peppas, Mechanisms of solute release from porous hydrophilic polymers, Int. J. Pharm. 15 (1983) 25–35. https://doi.org/10.1016/0378-5173(83)90064-9.

[63] J. Siepmann, N.A. Peppas, Modeling of drug release from delivery systems based on hydroxypropyl methylcellulose (HPMC), Adv. Drug Deliv. Rev. 64 (2012) 163–174. https://doi.org/10.1016/j.addr.2012.09.028.

[64] X. Zhao, Z. Wang, A pH-sensitive microemulsion-filled gellan gum hydrogel encapsulated apigenin: Characterization and in vitro release kinetics, Colloids Surfaces B Biointerfaces. 178 (2019) 245–252. https://doi.org/10.1016/j.colsurfb.2019.03.015.

[65] R. Gouda, H. Baishya, Z. Qing, Application of mathematical models in drug release kinetics of carbidopa and levodopa ER tablets, J. Dev. Drugs. 6 (2017).

[66] M. Ravi, S.R. Kaviya, V. Paramesh, Culture phases, cytotoxicity and protein expressions of agarose hydrogel induced Sp2/0, A549, MCF-7 cell line 3D cultures, Cytotechnology. 68 (2016) 429–441. https://doi.org/10.1007/s10616-014-9795-z.

[67] R.K. Mishra, M. Datt, A.K. Banthia, Synthesis and characterization of pectin/pvp hydrogel membranes for drug delivery system, AAPS PharmSciTech. 9 (2008) 395–403.

https://doi.org/10.1208/s12249-008-9048-6.
[68] T. Murata, T. Kutsuna, K. Kurohara, K. Shimizu, A. Tomeoku, N. Arai, Evaluation of a new hydroxyapatite nanoparticle as a drug delivery system to oral squamous cell carcinoma cells, Anticancer Res. 38 (2018) 6715–6720. https://doi.org/10.21873/anticanres.13040.
[69] J. Xu, P. Xu, Z. Li, J. Huang, Z. Yang, Oxidative stress and apoptosis induced by hydroxyapatite nanoparticles in C6 cells, J. Biomed. Mater. Res. - Part A. 100 A (2012) 738–745. https://doi.org/10.1002/jbm.a.33270.
[70] S. Ranganathan, D. Halagowder, N.D. Sivasithambaram, Quercetin suppresses twist to induce apoptosis in MCF-7 breast cancer cells, PLoS One. 10 (2015) 1–21. https://doi.org/10.1371/journal.pone.0141370.
[71] R. Meena, K.K. Kesari, M. Rani, R. Paulraj, Effects of hydroxyapatite nanoparticles on proliferation and apoptosis of human breast cancer cells (MCF-7), J. Nanoparticle Res. 14 (2012). https://doi.org/10.1007/s11051-011-0712-5.
[72] S. Balakrishnan, S. Mukherjee, S. Das, F.A. Bhat, P. Raja Singh, C.R. Patra, J. Arunakaran, Gold nanoparticles–conjugated quercetin induces apoptosis via inhibition of EGFR/PI3K/Akt–mediated pathway in breast cancer cell lines (MCF-7 and MDA-MB-231), Cell Biochem. Funct. 35 (2017) 217–231. https://doi.org/10.1002/cbf.3266.
[73] J.M. Manouchehri, K.A. Turner, M. Kalafatis, TRAIL-induced apoptosis in TRAIL-resistant breast carcinoma through quercetin cotreatment, Breast Cancer Basic Clin. Res. 12 (2018) 31–33. https://doi.org/10.1177/1178223417749855.
[74] C. Yu, C. Gao, S. Lü, C. Chen, Y. Huang, M. Liu, Redox-responsive shell-sheddable micelles self-assembled from amphiphilic chondroitin sulfate-cholesterol conjugates for triggered intracellular drug release, Chem. Eng. J. 228 (2013) 290–299. https://doi.org/10.1016/j.cej.2013.04.083.

Figure legends

Fig 1. Formation of a quercetin-loaded hydrogel nanocomposite with non-covalent interaction of nanoparticles and hydrogel.

Fig 2. Emulsion-based nanostructures as potential carriers in drug delivery. Oil in water (O/W) nanoemulsion (left) and water in oil in water (W/O/W) double emulsion (right) for the delivery of quercetin.

Fig 3. Preparation of the nanocomposite hydrogel and its encapsulation in the water in oil in water (W/O/W) double emulsion.

Fig 4. The FTIR spectra of PVP, AG-PVP, AG-PVP-HAp, and AG-PVP-HAp-QC.

Fig 5. The XRD patterns of PVP, AG-PVP, AG-PVP-HAp, and AG-PVP-HAp-QC.

Fig 6. FESEM image of freeze-dried hydrogel nanocomposites of AG-PVP-HAp loaded with quercetin.

Fig 7. Quercetin release profile for AG-PVP-HAp hydrogel at pH=5.4 and for nanocarriers encapsulating quercetin-loaded AG-PVP-HAp hydrogel nanocomposite and AG-PVP without HAp at pH 5.4 and 7.4

Fig 8. Cumulative release percent of quercetin at each time point for each group. Difference between pH 5.4 with HAp and all other groups is significant at $p < 0.001$(***).

Fig 9. Drug release data fitted to mathematical models of drug release.

Fig 10. In vitro cell cytotoxicity of free quercetin, quercetin loaded in AG-PVP and AG-PVP-

HAp, and AG-PVP-HAp against MCF-7 after 72 h incubation. Data are represented as mean ± SEM of three independent experiments in duplicate. Difference between control and AG-PVP-HAp is significant at $p<0.01$ (**). Difference between control and other groups is significant at $p < 0.001$(***). Difference between free quercetin and AG-PVP-QC is significant at $p< 0.05$($^{\$}$). Difference between free quercetin and AG-PVP-HAp is significant at $p< 0.01$($^{\$\$}$). Difference between free quercetin and AG-PVP-HAp-QC is significant at $p < 0.001$ ($^{\$\$\$}$). Difference between AG-PVP-QC and AG-PVP-HAp-QC is significant at $p < 0.001$ ($^{\#\#\#}$).

Fig 11. Flow cytometric analyses of apoptosis and necrosis in MCF-7 cells induced by free quercetin, quercetin loaded in AG-PVP and AG-PVP-HAp, and AG-PVP-HAp, using Annexin V-FITC and PI double staining. Quadrant analysis of fluorescence intensity of non-gated cells in FL1 (Annexin V) vs FL3 (PI) channels was from 5000 events. The values shown in the lower left, lower right, upper left, and upper right quadrants of each panel represent the percentage of viable, apoptotic, necrotic, and late apoptotic (post-apoptotic necrotic) cells, respectively.

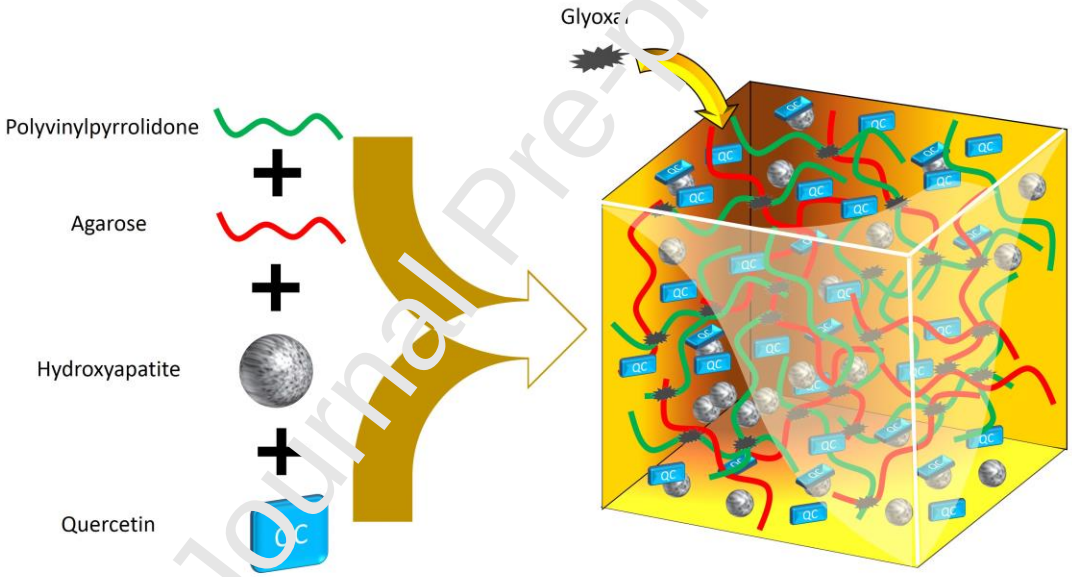

International Journal of Biological Macromolecules, Amirmasoud Samadi et al., Figure 1

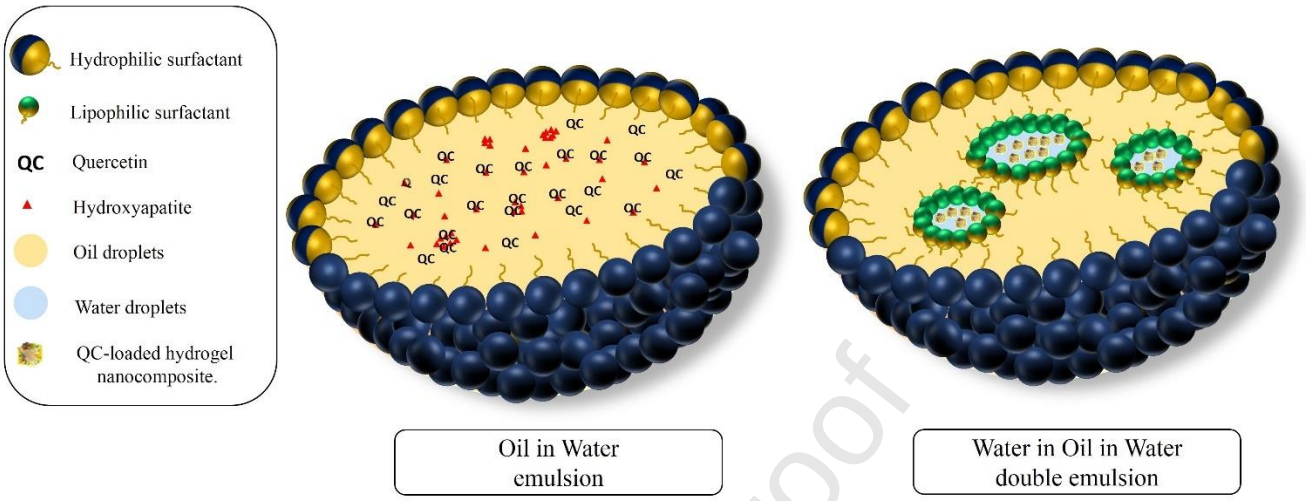

International Journal of Biological Macromolecules, Amirmasoud Samadi et al., Figure 2

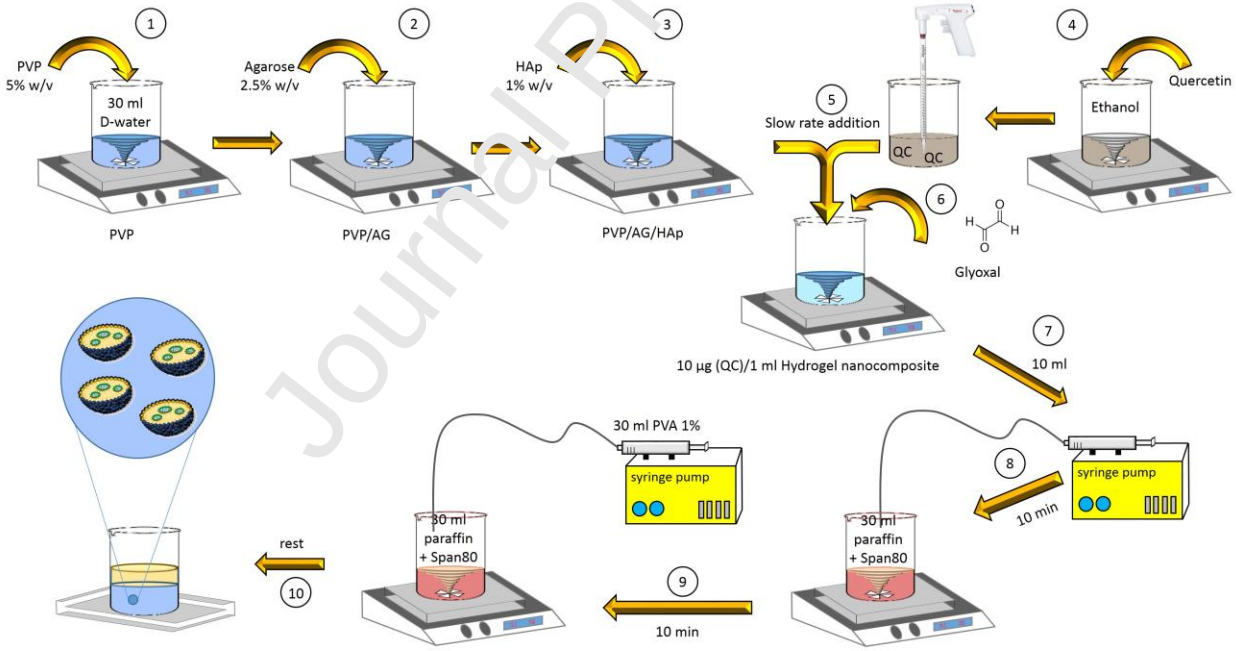

International Journal of Biological Macromolecules, Amirmasoud Samadi et al., Figure 3

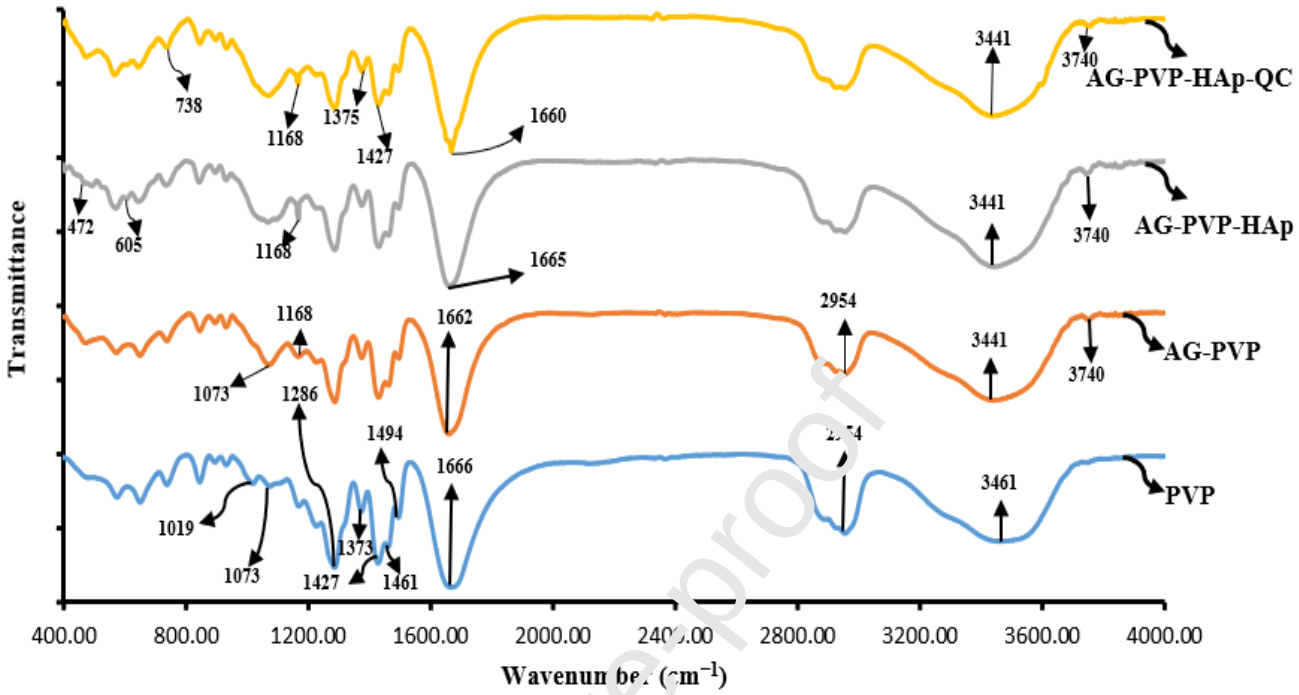

International Journal of Biological Macromolecules, Amirmasoud Samadi et al., Figure 4

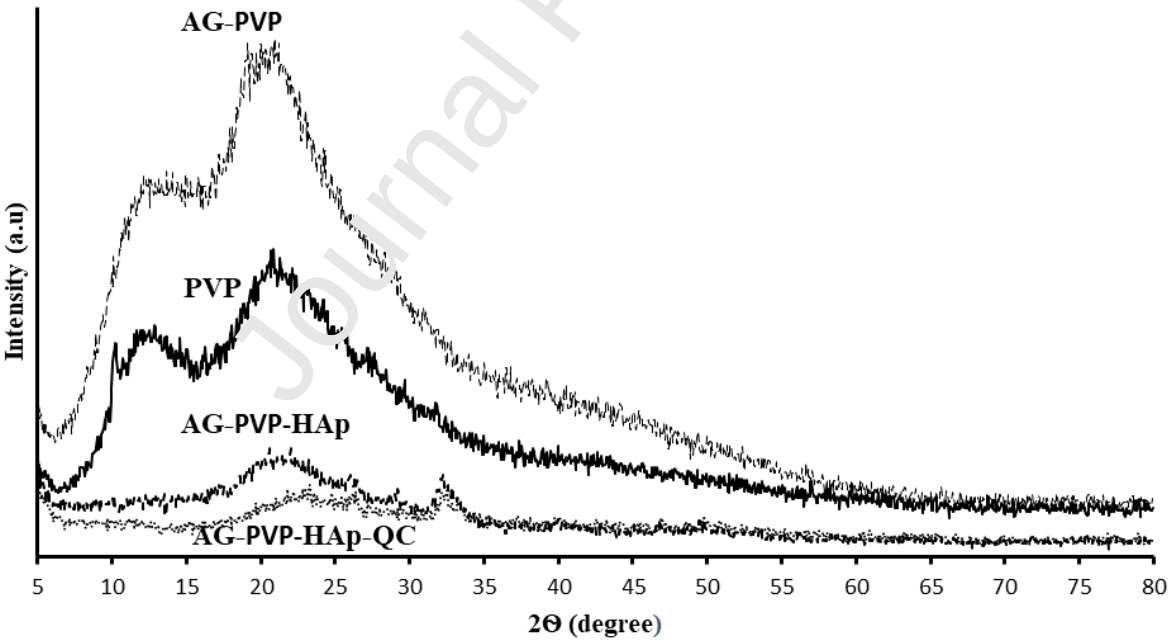

International Journal of Biological Macromolecules, Amirmasoud Samadi et al., Figure 5

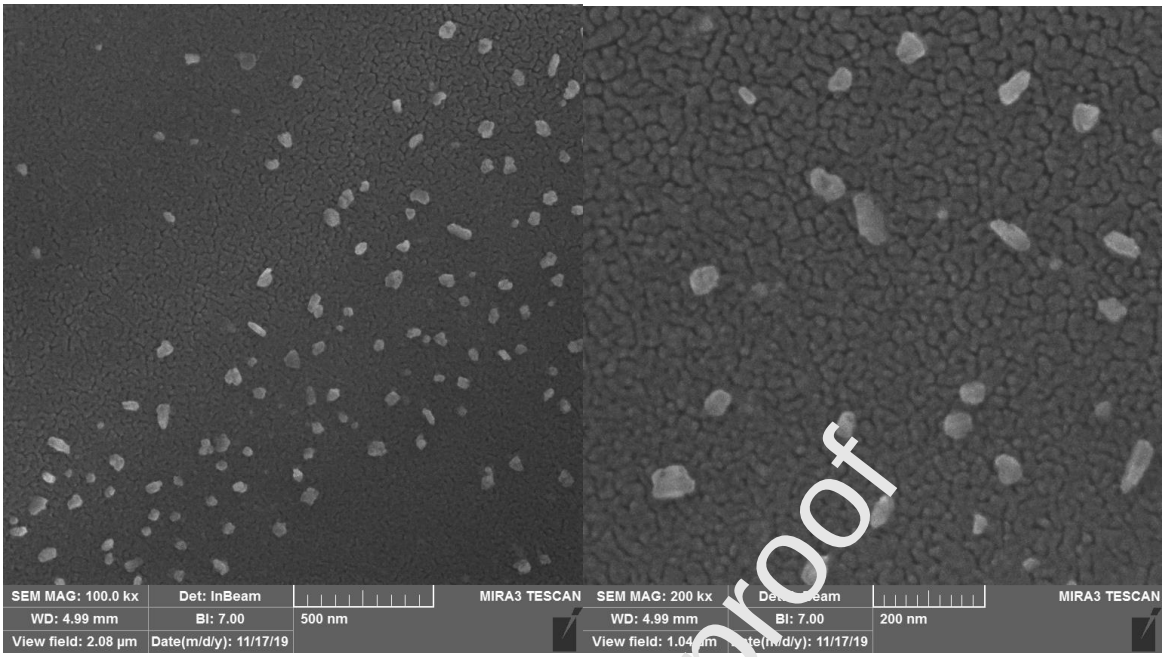

International Journal of Biological Macromolecules, Amirmasoud Samadi et al., Figure 6

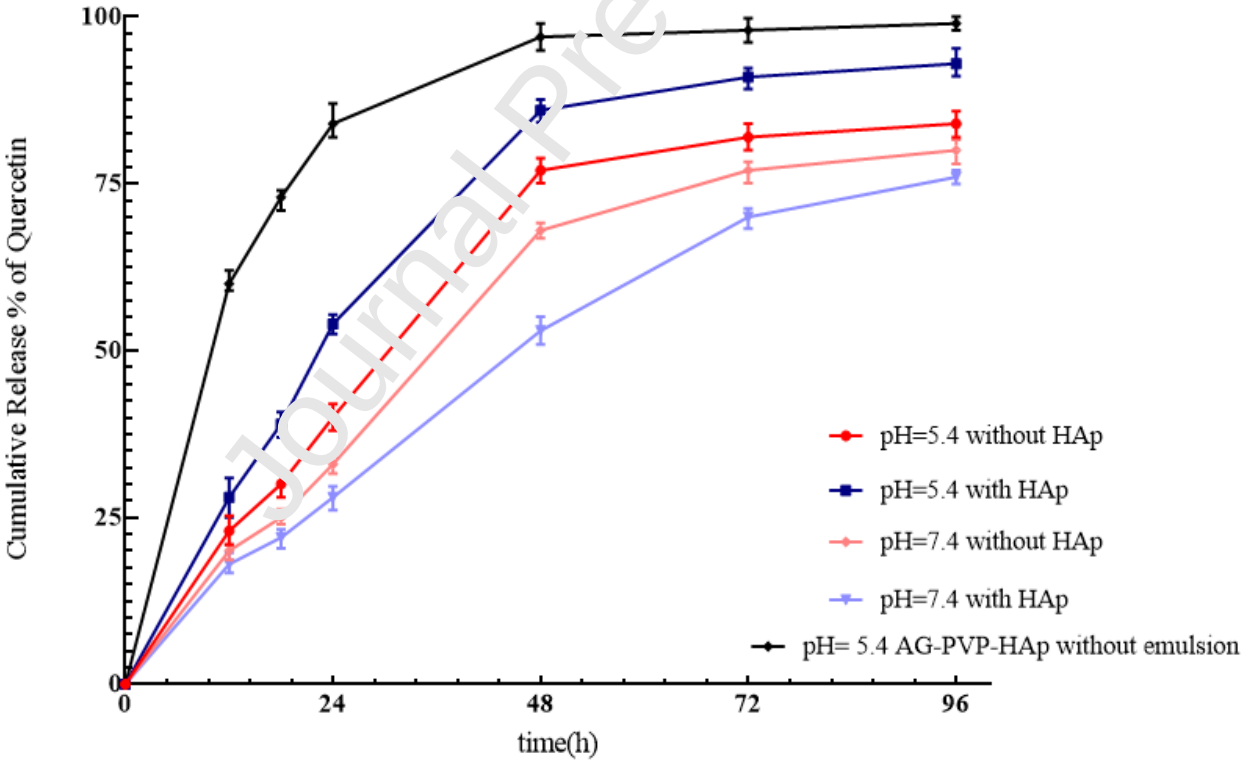

International Journal of Biological Macromolecules, Amirmasoud Samadi et al., Figure 7

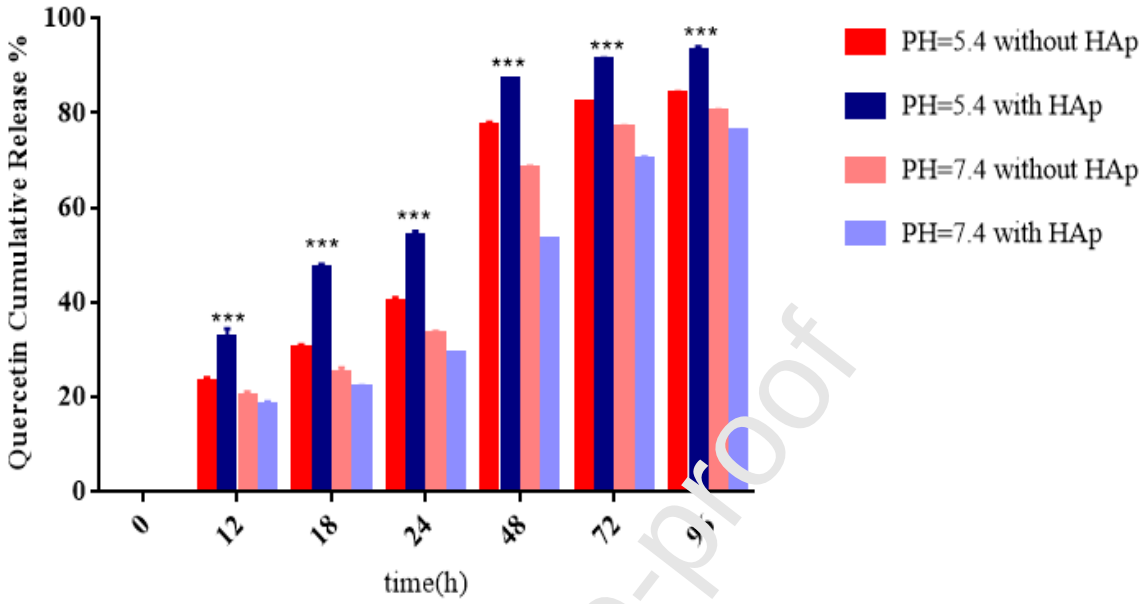

International Journal of Biological Macromolecules, Amirmasoud Samadi et al., Figure 8

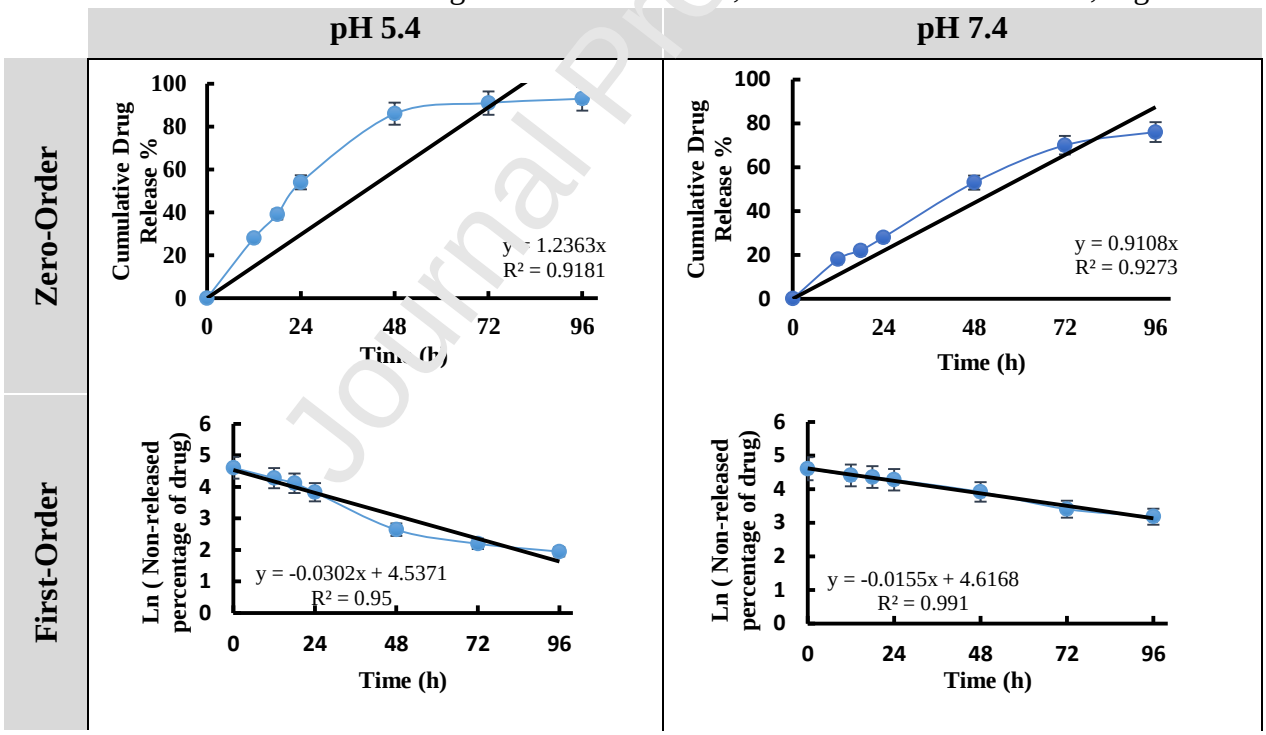

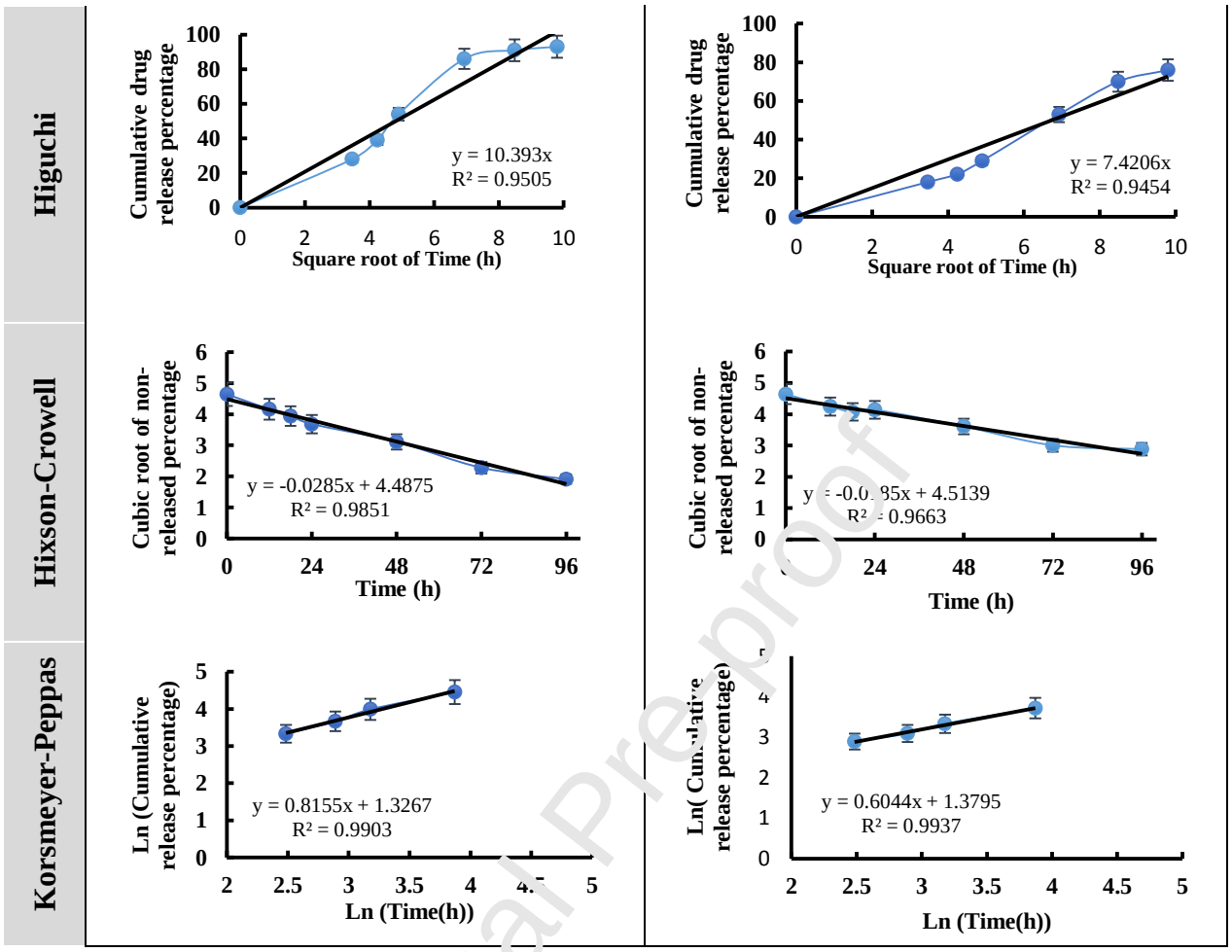

International Journal of Biological Macromolecules, Amirmasoud Samadi et al., Figure 9

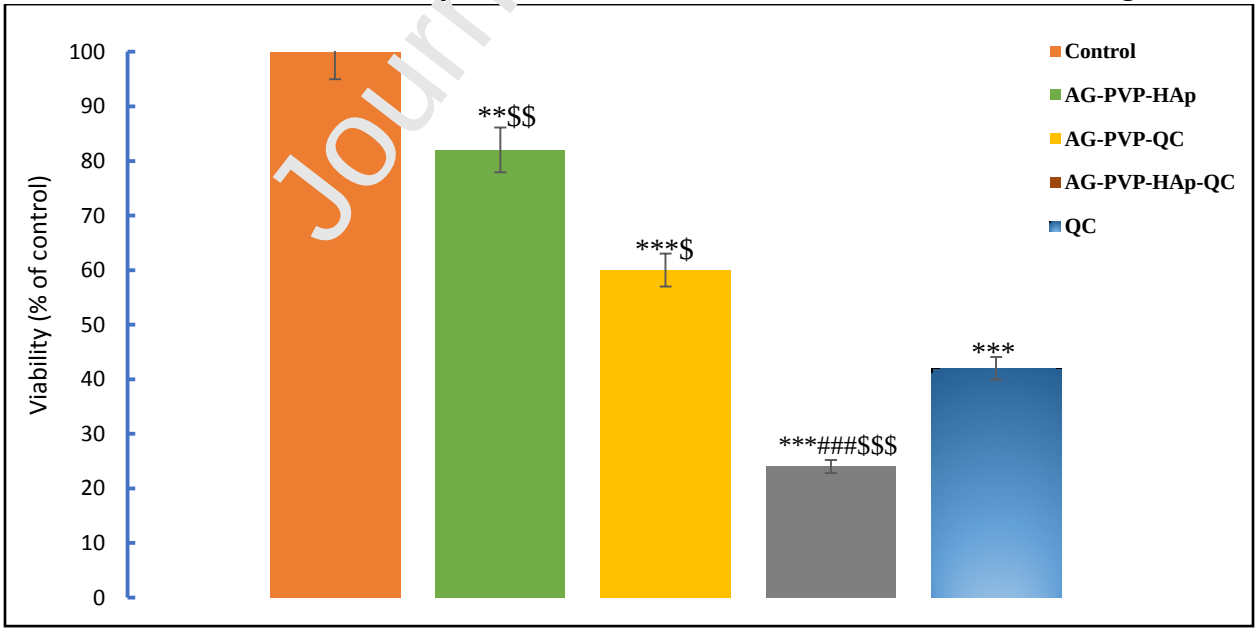

International Journal of Biological Macromolecules, Amirmasoud Samadi et al., Figure 10

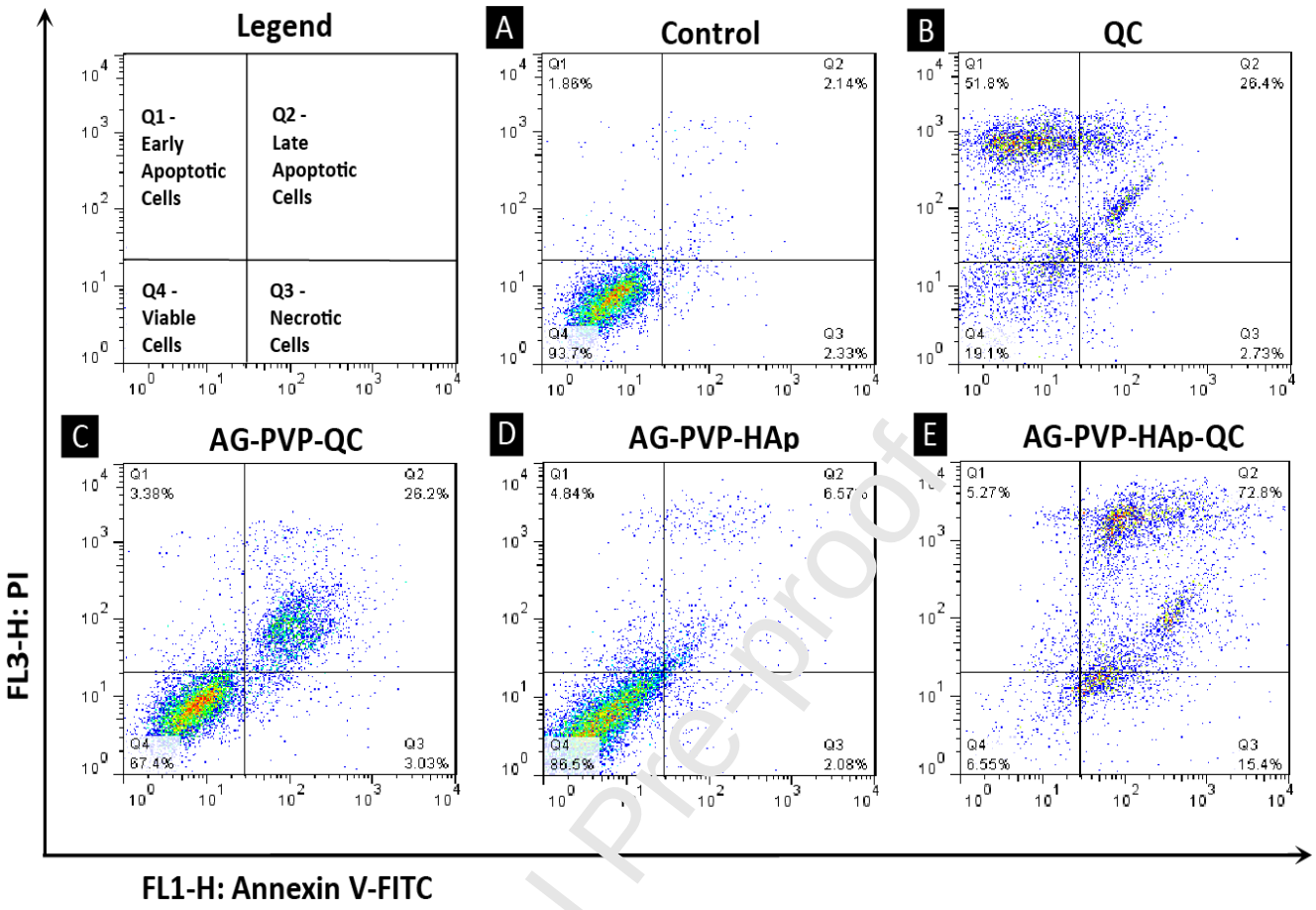

International Journal of Biological Macromolecules, Amirmasoud Samadi et al., Figure 11

Table 1. Effect of HAp on quercetin drug loading and encapsulation efficiencies.

	AG-PVP	AG-PVP-HAp	Effect of HAp (%)
Loading (%)	48	61	+13
Encapsulation (%)	85	93	+8

Table 2. Encapsulation and loading efficiencies reported in former studies and the current study

Drug delivery platforms for quercetin delivery	Loading %	Encapsulation %	Reference
Chitosan–quinoline nanoparticles	9.6	77	[52]
Graphene oxide (GO)- polyvinylpyrrolidone (PVP)	20	----------	[53]
Quercetin liposomes	2.58	68.2	[7]
Solid lipid nanoparticles (SLN)	16.65	83.27	[54]
Nano lipidic carriers (NLC)	17.98	89.91	[54]
Shell-sheddable micelles	23.4	30.6	[74]
Cationic nanostructured lipid carriers	3.95	89.3	[55]

Quercetin conjugated Fe_3O_4 nanoparticles (QCMNPs)	6.08	81.6	[56]
QC-loaded AG-PVP-HAp nanocomposite encapsulated in double emulsion	61	93	This work

Table 3. Kinetic modeling of drug release.

	Model	Equation	R^2
	Zero-order	$C_t = 0.9108\ t$	0.9764
	First-order	$ln\ (1-\frac{M_t}{M_\infty}) = 4.6168 - 0.0155\ t$	0.9910
pH=7.4	Higuchi	$Q = 7.4206\ t^{\frac{1}{2}}$	0.9824
	Hixson-Crowell	$(1-\frac{M_t}{M_\infty})^{\frac{1}{3}} = 4.5139 - 0.0185\ t$	0.9663
	Korsmeyer-Peppas	$ln(\frac{M_t}{M_\infty}) = 0.6044\ ln\ t + 1.3795$	0.9937
	Zero-order	$C_t = 1.2363\ t$	0.9181
	First-order	$ln\ 1-\frac{M_t}{M_\infty}) = 4.5371 - 0.0302\ t$	0.9500
pH=5.4	Higuchi	$Q = 10.393\ t^{\frac{1}{2}}$	0.9871
	Hixson-Crowell	$(1-\frac{M_t}{M_\infty})^{\frac{1}{3}} = 4.4875 - 0.0285\ t$	0.9851
	Korsmeyer-Peppas	$ln(\frac{M_t}{M_\infty}) = 0.8155\ ln\ t + 1.3267$	0.9903

Declaration of Interest

The authors declare that there is no conflict of interest.

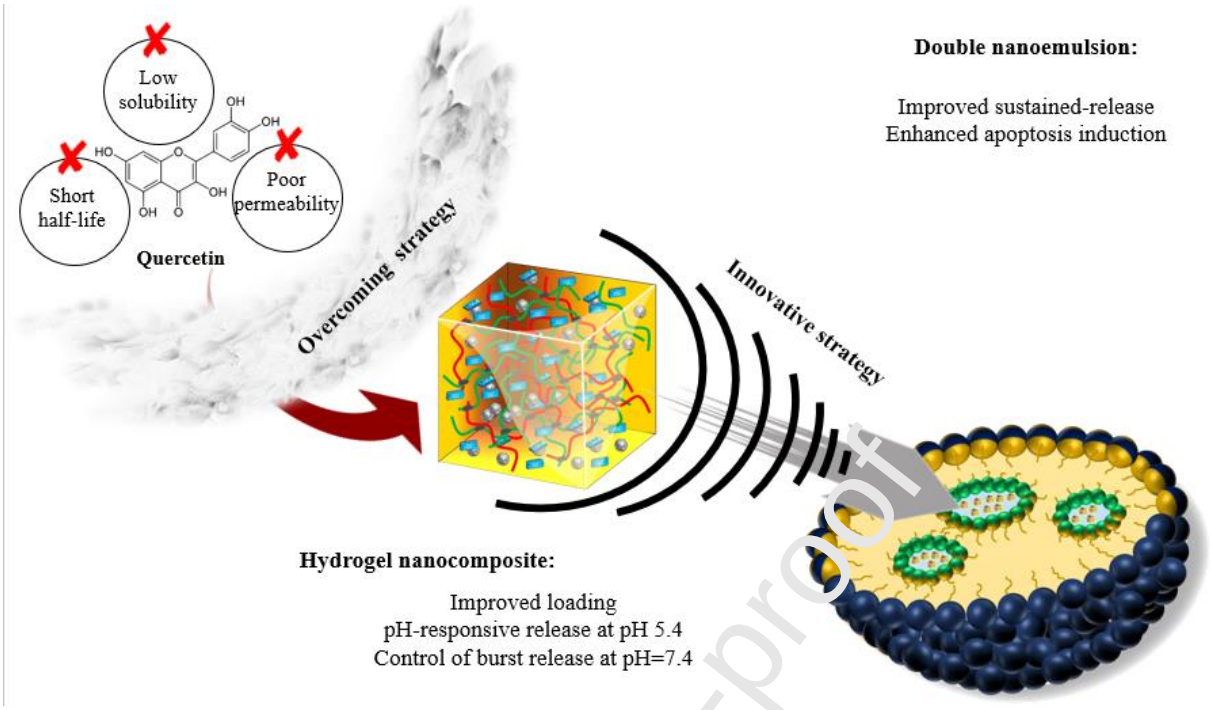

Graphical abstract